Bioactive Materials 41 (2024) 640–656

Contents lists available at ScienceDirect

Bioactive Materials

journal homepage: www.keaipublishing.com/en/journals/bioactive-materials

Suspension electrospinning of decellularized extracellular matrix: A new method to preserve bioactivity

Sarah Jones [a], Sabrina VandenHeuvel [b], Andres Luengo Martinez [a], Ruchi Birur [a], Eric Burgeson [c], Isabelle Gilbert [a], Aaron Baker [a], Matthew Wolf [d], Shreya A. Raghavan [b], Simon Rogers [c], Elizabeth Cosgriff-Hernandez [a,*]

[a] Department of Biomedical Engineering, The University of Texas at Austin, Austin, TX, 78712, USA
[b] Department of Biomedical Engineering, Texas A&M University, College Station, TX, 77843, USA
[c] Department of Chemical and Biomolecular Engineering, University of Illinois Urbana-Champaign, Champaign, IL, 61820, USA
[d] Cancer Biomaterials Engineering Section, Cancer Innovation Laboratory, Center for Cancer Research, National Cancer Institute, Frederick, MD, 21702, USA

ARTICLE INFO

Keywords:
Electrospinning
Extracellular matrix
Biological scaffolds

ABSTRACT

Decellularized extracellular matrices (dECM) have strong regenerative potential as tissue engineering scaffolds; however, current clinical options for dECM scaffolds are limited to freeze-drying its native form into sheets. Electrospinning is a versatile scaffold fabrication technique that allows control of macro- and microarchitecture. It remains challenging to electrospin dECM, which has led researchers to either blend it with synthetic materials or use enzymatic digestion to fully solubilize the dECM. Both strategies reduce the innate bioactivity of dECM and limit its regenerative potential. Herein, we developed a new suspension electrospinning method to fabricate a pure dECM fibrous mesh that retains its innate bioactivity. Systematic investigation of suspension parameters was used to identify critical rheological properties required to instill "spinnability," including homogenization, concentration, and particle size. Homogenization enhanced particle interaction to impart the requisite elastic behavior to withstand electrostatic drawing without breaking. A direct correlation between concentration and viscosity was observed that altered fiber morphology; whereas, particle size had minimal impact on suspension properties and fiber morphology. The versatility of this new method was demonstrated by electrospinning dECM with three common decellularization techniques (Abraham, Badylak, Luo) and tissue sources (intestinal submucosa, heart, skin). Bioactivity retention after electrospinning was confirmed using cell proliferation, angiogenesis, and macrophage polarization assays. Collectively, these findings provide a framework for researchers to electrospin dECM for diverse tissue engineering applications.

1. Introduction

Tissue engineering scaffolds composed of decellularized extracellular matrices (dECM) have shown a tremendous capacity to support regeneration in numerous applications [1]. The dECM guides tissue remodeling by providing structural and biological cues with its complex composition of fibrous proteins, proteoglycans, growth factors, cytokines, and mRNA [1–4]. Cells interact with and resorb the dECM, leading to the release of bioactive products, such as chemoattractive low molecular weight proteins, angiogenic growth factors, and mRNA [1,4,5]. Tissue-specific dECM has successfully promoted angiogenic, myogenic, neurogenic, and immunomodulatory behavior by supporting cell recruitment, proliferation, and tissue-specific differentiation [6–12]. Small intestinal submucosa (SIS) is one of the most prominent dECM scaffolds on the market because it contains the high levels of growth factors and nutrients necessary to support the continual regeneration of the intestinal lining. SIS scaffolds have shown success in regenerating airway [13], abdominal wall [14,15], diaphragm [16], intestine [17], bladder [18], rotator cuff [19], skin [20–22], and urethra [23] tissue in clinical trials [1].

Peer review under responsibility of KeAi Communications Co., Ltd.
* Corresponding author.
E-mail addresses: sk.jones@utexas.edu (S. Jones), snvh@tamu.edu (S. VandenHeuvel), luengoad@utexas.edu (A. Luengo Martinez), ruchibirur@utexas.edu (R. Birur), ericmb3@illinois.edu (E. Burgeson), gilbert@utexas.edu (I. Gilbert), abbaker@austin.utexas.edu (A. Baker), matthew.wolf@nih.gov (M. Wolf), sraghavan@tamu.edu (S.A. Raghavan), sarogers@illinois.edu (S. Rogers), cosgriff.hernandez@utexas.edu (E. Cosgriff-Hernandez).

https://doi.org/10.1016/j.bioactmat.2024.08.012
Received 26 April 2024; Received in revised form 12 August 2024; Accepted 14 August 2024

Fabrication of dECM into specialized structures for a target application remains challenging. The bioactivity of proteins and growth factors can be easily deactivated with enzymatic digestion, heat exposure, or harsh solvents [24]. Clinical practice is currently limited to native form sheets of dECM [4,7]. The macroscopic structure and microscopic morphology of dECM scaffolds are constrained to the structure of the harvested tissue, likely sheets or tubes. Current research strategies to expand the application of dECM scaffolds have been exploring hydrogels and combination devices like coatings and composites [4]. Hydrogels provide a swollen matrix with the potential for injection [6,25,26]. However, gel fabrication requires enzymatic digestion to solubilize the ECM, which can denature and deactivate important components reducing the functional bioactivity of the dECM [27,28]. Similarly, dECM coatings and composites can have improved mechanical properties or structures, but they contain alternative materials that can alter the foreign body reaction and tissue remodeling response [29–32]. A method is needed to produce dECM scaffolds with retained bioactivity, the ability to modulate geometry, and without additive materials that can produce negative biological responses.

Electrospinning is a fabrication platform that allows control of macro- and micro-architecture and can be scaled to fabricate meshes with clinically relevant dimensions. For example, electrospun materials can be fabricated with complex macrostructures such as valves, grafts, dressings, and wraps. Additionally, fiber microarchitecture can be controlled to vary anisotropy, pore size, and surface texture [10,33–38]. For instance, the fibers can be aligned to support the regeneration of anisotropic tissues like skeletal muscle or randomly oriented to support the regeneration of isotropic tissue like adipose tissue. The interconnected porosity and high surface area of electrospun meshes also provide a tunable platform for cell interaction and infiltration. Although electrospinning shows promise for dECM scaffold fabrication with high bioactivity retention and versatile structure, it remains common to use polymeric additives to facilitate fiber formation of dECM while electrospinning [39–48]. Conventional electrospinning requires the mobility of polymeric chains for alignment along the electrostatic field and chain entanglement to withstand the electrostatic forces [49]. The polymeric additives provide increased chain entanglement; however, additives can negatively alter the biological response to the scaffold [29,30]. Other methods to enhance spinnability utilize enzymatic digestion to break down the ECM into individual chains, which can reduce bioactivity through denaturation [27,28]. In contrast with traditional spinning solutions of digested and dissolved dECM, our recent work showcased a new suspension electrospinning method using decellularized skeletal muscle. The resulting scaffold retained myogenic bioactivity as indicated by cell attachment, proliferation, and differentiation [10,50]. Electrospinning ECM suspensions, without complete digestion, has the potential to maintain higher orders of protein structure which can translate into ECM scaffolds with a higher retention of bioactivity and slower resorption rates. Control and extension of ECM scaffold resorption could abrogate the need for chemical crosslinking agents that impair remodeling and induce a chronic foreign body response. However, electrospinning of dECM suspensions is in its nascency, and thus critical rheological parameters to obtain a spinnable suspension have yet to be elucidated [10,50,51]. A rigorous evaluation of suspension properties and their capacity for fiber formation is needed to expand the use of electrospun dECM scaffolds to a wide range of tissue engineering applications.

In this study, the critical properties of dECM suspensions that are required to facilitate electrospinning, or instill "spinnability," are identified. We conducted a rigorous rheological evaluation of a wide range of dECM suspensions fabricated with varying homogenization levels, concentrations, and ground particle sizes with dECM derived from SIS. The versatility of the dECM suspension electrospinning method is showcased by electrospinning different ECM compositions, either prepared with different decellularization techniques or tissue sources. The level of bioactivity retention was then assessed via cell proliferation, macrophage polarization, and angiogenesis. This assessment of the critical parameters involved in electrospinning dECM aims to provide an accessible toolbox for research groups to create specialized dECM scaffolds with high bioactivity retention for numerous tissue regeneration applications.

2. Materials and methods

2.1. Materials

All materials were purchased from Sigma Aldrich unless otherwise noted.

2.2. Small intestinal submucosa isolation

The submucosal layer of a 6–9 month porcine small intestine (Animal Technologies) was isolated as previously described [52]. The small intestine was washed in PBS and cut into 10 cm sections. Each section was sliced longitudinally to form a flat sheet. The outer layer comprised of the serosa and muscularis externa was mechanically delaminated, and the inner mucosa layer was removed with repeated mechanical shearing. The remaining layer is the SIS. The SIS was stored in PBS at 4 °C for no more than 24 h before beginning decellularization and preparation.

2.3. Tissue decellularization and preparation

Each SIS decellularization and preparation technique explored has been named the Abraham [53], Badylak [54,55], and Luo [6,56] technique based on the prior work. For the *Abraham technique* [53], 10 cm SIS sections were first submerged in 5 mL of 100 mM ethylenediaminetetraacetic acid (EDTA) in 10 mM sodium hydroxide (NaOH) for 16 h. Second, the SIS was transferred to 5 mL of 1M hydrochloric acid (HCl) in 1M sodium chloride (NaCl) for 8 h. Third, the SIS was transferred to 5 mL of 1M NaCl in 1X PBS for 16 h. Fourth, the SIS was transferred to 5 mL of 1X PBS for 2 h. Lastly, the SIS was transferred to 5 mL of DI water for 2 h. All biological composition and cell studies used SIS prepared with the Abraham technique. For the *Badylak technique* [54,55], 10 cm SIS sections were first submerged in 5 mL of 0.1 % peracetic acid and 4 % ethanol for 2 h. Second, the SIS was transferred to 5 mL of PBS for 15 min. Third, the SIS was transferred to 5 mL of DI water for 15 min. Fourth, the DI water was exchanged for another 15 min. For the *Luo Technique* [6,56], 10 cm SIS sections were each submerged in 5 mL of 1:1 methanol and chloroform for 12 h and subsequently washed with DI water. Second, the SIS was transferred to 5 mL of 0.05 % Trypsin-EDTA for 12 h and subsequently washed with saline. Third, the SIS was transferred to 5 mL of 0.5 % sodium dodecyl sulfate (SDS) in 0.9 % NaCl for 4 h and subsequently washed in saline. Fourth, the SIS was transferred to 5 mL of 0.1 % peracetic acid and 20 % ethanol for 30 min and subsequently rinsed with saline. During each step of the three different decellularization and preparation techniques, the SIS was continuously agitated at 37 °C. The prepared SIS was stored at −80 °C until further use. The native SIS was washed in 1X PBS without additional chemical treatment and stored at −80 °C until further use. Decellularization following each technique was confirmed via DNA quantification. The DNA of the SIS was extracted following the manufacturer's recommended protocol of the DNEasy Blood and Tissue Kit (Qiagen) and quantified with the Quant-iT™ PicoGreen™ dsDNA Assay Kit (ThermoFisher Scientific). There were 9 samples (n = 9) in each group done in triplicate. The DNA content within the decellularized tissue was confirmed to be less than 50 ng/mg of dried tissue before use in experiments, Fig. S3.

A 6–9 month porcine heart (Animal Technologies) was sectioned into 0.5 cm^3 pieces and prepared using the Badylak technique in 4 L of each medium described above with constant stirring. Skin tissue was isolated from Sprague Dawley rats. The hair was removed with Nair™ Hair

Remover. The skin was sectioned into 10 cm^2 pieces and prepared using the Abraham technique in 5 mL/piece of each medium described above. The prepared heart- and skin-derived ECM were stored at −80 °C until further use.

2.4. Preparation of dECM suspensions

Electrospinning suspension preparation is represented in Fig. 1A. The frozen prepared SIS-derived ECM was submerged in DI water and thawed at 37 °C. The SIS sheets were then homogenized with an OMNI Tissue Homogenizer TH (OMNI International). The homogenized SIS was flash-frozen in liquid nitrogen and lyophilized for 2 days. The dried SIS was broken into particles with an electric blade grinder (Kaffe) and separated into groups of <250 μm, 250–500 μm, 500–2000 μm, and >2000 μm with a sieve tower. SIS particles were suspended in chilled hexafluoroisopropanol (HFIP) at 10–60 mg/mL concentrations and allowed to mix for over 12 h at 4 °C. Immediately prior to electrospinning, the SIS suspensions were loaded into a capped syringe and homogenized for 20 s. The frozen prepared SIS sheets that were not homogenized were lyophilized immediately and then followed the same protocol as the dried SIS described above. The SIS suspensions that were not homogenized were transferred to a syringe and immediately electrospun. The skin-derived ECM suspension was prepared similarly with 500–2000 μm dried particle size, 70 mg/mL concentration, and both homogenization steps. The heart-derived ECM suspension was prepared similarly with 500–2000 μm dried particle size, 55 mg/mL concentration, and both homogenization steps.

2.5. Rheological assessment

The dECM suspensions were analyzed on a Discovery Hybrid Rheometer, DHR-3 (TA instruments) with a 25 mm parallel plate geometry. Descending and ascending strain amplitude sweeps between 0.1 and 1000 % strain were conducted at a constant angular frequency of 1.0 rad/s at 25 °C to identify the amplitude dependence of the storage and loss modulus of the dECM suspensions. The crossover points of the storage and loss modulus curves were identified with linear interpolation. A flow ramp was conducted between shear rates of 0.1–1000 s^{-1} at 25 °C to determine the rate-dependent viscosity of the dECM suspensions (n = 3). A visual assessment of the particles in suspension contributing to the variations in rheological behavior was conducted. The SIS suspensions were diluted 10-fold to 4 mg/mL in HFIP. To prepare for imaging, 20 μL of the diluted suspension was placed between 2 coverslips and imaged immediately before drying on a Nikon TS-100 brightfield microscope. Three samples were analyzed for each group with 5 images taken of each specimen (n = 15).

2.6. Electrospinning

The dECM suspensions were pumped from a 20 G needle charged with 18 kV at a flow rate of 0.5 mL/h (Fig. 1B). A grounded copper plate covered in parchment paper was placed 20 cm from the needle tip. Electrospinning progressed for 30 min for a single layer of fibers or for up to 8 h until the mesh reached the target thickness for assays. To prepare for imaging, the meshes were coated with 5 nm of gold (Sputter Coater 108, Cressington Scientific Instruments). The meshes were subsequently visualized with scanning electron microscopy (SEM, Phenom Pro, NanoScience Instruments, Phoenix, AZ) at an accelerating voltage of 10 kV. Three specimens were taken from each run with 5 micrographs taken of each specimen in a raster pattern (n = 15). The fiber diameter distribution was determined by measuring 100 fibers in each mesh with ImageJ® Software. The polydispersity index (PDI) was calculated as $(\sigma/\alpha)^2$, where σ is the standard deviation and α is the mean fiber diameter [57].

2.7. Thermal denaturation profile

The thermal denaturation profiles of SIS samples were determined with differential scanning calorimetry (DSC 2500, TA Instruments) as a means to assess the effect of electrospinning on protein denaturation. Native SIS sheets, decellularized SIS sheets, and electrospun SIS meshes were compared to positive controls of heat-treated SIS and native SIS sheets undergoing a second heating cycle. Each sample was cut to 5 mg and sealed in hermetic pans. A single heating cycle was performed from −20 to 200 °C at a rate of 5 °C/min. To prepare a heat-treated positive control for partial denaturation, SIS was submerged in 70 °C DI water for 1 h with constant mixing. A 2nd cycle thermogram of the native SIS was used as a second positive control with full denaturation occurring in the first heating cycle. The onset temperature (T_{onset}), peak temperature (T_{peak}), and enthalpy of denaturation (ΔH) were measured from the

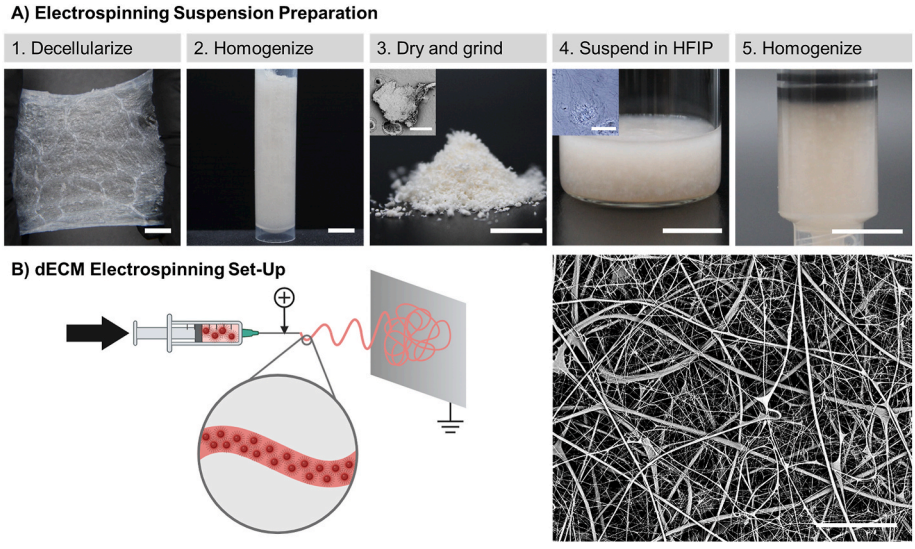

Fig. 1. Schematic of electrospinning method for dECM. A) The preparation of a dECM electrospinning suspension is a five-step process involving decellularization, homogenization, milling, suspension in HFIP, and a second round of homogenization. Macro images for steps 1–5; scale bar = 1 cm. Inset SEM image of dried SIS particle in step 3; scale bar = 300 μm. Inset brightfield image of suspended SIS particle in step 4; scale bar = 60 μm. B) The dECM suspension is electrospun by applying an electric field between the flowing suspension and a collector. Graphic created in BioRender. SEM image of electrospun dECM fibers; scale bar = 30 μm.

thermogram using TRIOS software (TA Instruments). T_{onset} was calculated as the intersection of the tangent to the heat flow baseline. T_{peak} was calculated as the temperature with the minimum heat flow value. Lastly, ΔH was calculated as the area between the heat flow curve and the tangent line of the heat flow baseline. Representative thermograms are presented with average thermal transitions reported (n = 3).

2.8. Biochemical composition

The total protein, collagen, and sulfated glycosaminoglycan (sGAG) content of the native, decellularized, and electrospun SIS samples were analyzed. For *total protein analysis*, the bicinchoninic acid (BCA) Protein Assay Kit II (BioVision) was used. The lysing buffer was prepared with 1 mg/mL proteinase K (Qiagen) in 50 mM Tris-HCl and 5 mM $CaCl_2$. Dried SIS samples were lysed in the lysing buffer at a concentration of 15 mg/mL at 50 °C shaking at 150 rpm overnight. Reagent A + B was prepared with a 50:1 A to B ratio. The BCA Reagent A + B was added to the lysed samples at an 8:1 ratio and vortexed. The absorbance was measured on a plate reader (Infinite M Nano+, Tecan) at a wavelength of 562 nm. A standard curve was generated with bovine serum albumin from a concentration of 0–2000 μg/mL. For *collagen analysis*, a hydroxyproline assay was used as previously described [58]. The lysing buffer was prepared with 1 mg/mL proteinase K (Qiagen) in 50 mM Tris-HCl and 5 mM $CaCl_2$. Dried SIS samples were lysed in the lysing buffer at a concentration of 10 mg/mL at 60 °C shaking at 200 rpm overnight. The samples were hydrolyzed by adding 100 μL 10 M NaOH to 100 μL of the lysed samples and autoclaving for 15 min at 121 °C. Samples were neutralized with 10 M HCl. Chloramine-T solution was prepared with 342 mg Chloramine-T, 755 mg NaOH, 807 mg citric acid, 1115 mg sodium acetate, 193 μL acetic acid, 7.8 mL isopropanol, and 22.2 mL ultrapure water. Samples were oxidized by adding 625 μL of chloramine-T solution and incubating for 20 min at room temperature. Ehrlich's solution was prepared with 1790 mg P-dimethyl-amino-benzaldehyde (DMAB) in 30 % HCl and 70 % isopropanol. To initiate color change, 625 μL of Ehrlich's solution was added and samples were submerged in a 60 °C water bath for 20 min. The absorbance was measured on a plate reader (Infinite M Nano+, Tecan) at a wavelength of 560 nm. A standard curve was generated with collagen from bovine achilles tendon from a concentration of 0–40 mg/mL. For *sGAG analysis*, a 1,9-dimethylmethylene blue (DMMB) assay was used as previously described [50]. Dried SIS samples were lysed as in the BCA assay. Formate solution was prepared with 104 mg of sodium formate, 10 mL of 1 M guanidine hydrochloride, and 116 μL of 85 % formic acid. A 1.53 μM DMMB solution was prepared in ethanol. The working solution was prepared with 5 mL of formate solution, 1.25 DMMB solution, and 18.75 mL ultrapure water. The working solution was added to the lysed samples at a 5:1 vol ratio and mixed for 30 min at 150 rpm. The samples were centrifuged at 15,000 rpm for 10 min. The supernatant was decanted, and the sGAG-dye complex precipitate was isolated. A decomplexation solution was prepared with 82 mg sodium acetate, 2 mL isopropanol, 10 mL 8 M guanidine hydrochloride, and 8 mL ultrapure water. The decomplexation solution was added to the precipitate at a 5:1 ratio to the original lysed sample volume and vortexed. The absorbance was measured on a plate reader (Infinite M Nano+, Tecan) at a wavelength of 656 nm. A standard curve was generated with chondroitin-4-sulfate from a concentration of 0–100 μg/mL. Samples were run in triplicate for each assay with 3 specimens per group (n = 9).

2.9. Cell proliferation

The bioactivity retention and cytotoxicity of SIS after electrospinning was first analyzed via cell proliferation. To minimize the risks of utilizing an HFIP solvent system that is known to be cytotoxic, the ECM meshes were vacuum-dried to remove any residual solvent after electrospinning. Electrospun SIS meshes and decellularized SIS sheets were cut into 8 mm discs and sterilized with UV irradiation for 15 min on each side. Human dermal fibroblasts (hDFs) were expanded in alpha minimum essential media (α-MEM) growth media, supplemented with 10 % fetal bovine serum (Atlanta Biologicals, Flowery Branch, GA) and 1 % of penicillin-streptomycin (10,000 U/mL, Thermo Fisher Scientific) at 37 °C and 5 % CO_2. The cells were seeded on the surface of the SIS samples at 25,000 cells/cm^2 and cultured for 1, 3, 5, and 7 days at 37 °C and 5 % CO_2. The hDF metabolic activity was measured with the CellTiter 96 ® Aqueous MTS Kit (Promega Corp., Madison, WI, USA). At each timepoint, the samples were removed from the cell media and incubated with 17 % (v/v) CellTiter 96 ® Aqueous One Solution Reagent diluted in media at 37 °C and 5 % CO_2 for 1 h. Subsequently, the absorbance of 100 μL of the media was analyzed on a plate reader (Infinite M Nano+, Tecan) at a wavelength of 490 nm. Biological duplicates of each sample were performed with three specimens in each group (n = 6).

2.10. Angiogenic assays: in vitro tube formation and chorioallantoic membrane (CAM) assay

A tube formation assay was performed to evaluate the angiogenic capacity of the releasate from SIS samples per standard protocol [59]. Basal media (Endothelial Basal Medium 2 with 0.5 % fetal bovine serum, Fisher Scientific) was conditioned with a decellularized SIS sheet, electrospun SIS mesh, and vascular endothelial growth factor (VEGF) positive control. Non-conditioned basal media was used as a negative control. To prepare the SIS-conditioned media, dried 5 mg SIS samples were sterilized with UV irradiation and soaked in 1 mL of basal media at 4 °C for 7 days with constant agitation. To prepare the VEGF-conditioned media, recombinant human VEGF (R&D Systems) was added to the basal media at 20 ng/mL immediately prior to cell treatment. Human umbilical vein endothelial cells (HUVECs) were expanded in Endothelial Growth Medium 2 (Fisher Scientific) until confluent. The HUVECs were starved for 24 h in basal media prior to the tube formation assay. Reduced Growth Factor Matrigel (Corning) was plated in a 96-well plate (50 μL per well) and incubated at 37 °C for 30 min. HUVECs were seeded directly on the Matrigel at 40,000 cells/well in 25 μL of basal media, and 300 μL of the corresponding conditioned media was added immediately. The HUVECs were incubated at 37 °C for 4 h. HUVECs were stained with Calcein-AM (Biotium) diluted to 1:2000 for 30 min and imaged with a fluorescent microscope (Nikon TS-100). The number of networks formed in each media group per image were manually counted. Samples were run in triplicate with 5 images taken of each specimen (n = 15).

A chorioallantoic membrane (CAM) assay was used to measure the angiogenic capacity of SIS samples. The samples tested include a decellularized SIS sheet, an electrospun SIS mesh, and a 200 μm Nylon mesh negative control. Fertilized Japanese quail eggs (Southwest Gamebirds) were incubated horizontally at 37 °C and 50 % relative humidity for 3 days. The eggshells were sterilized with 70 % ethanol and allowed to dry. The embryo was removed from the shell and placed in a 50 mm Petri dish. Three 50 mm polystyrene dishes were placed in a 150 mm Petri dish filled with 5 mL DI water to maintain a 100 % humid environment and incubated at 37 °C for 7 days. The samples were cut to 6 mm discs and placed 2–3 mm to the side of the central anterior vitelline vein in the outer third of the CAM as previously described [60]. Images were taken daily for 4 days with a stereoscope to visualize angiogenesis. Vessel density was quantified as the change in the number of vessels crossing the outer perimeter of the sample from Day 0 to Day 4 (n = 5).

2.11. Macrophage polarization assay

Gene expression of macrophages cultured on SIS samples was analyzed to evaluate the retention of immunomodulatory bioactivity after electrospinning [61]. THP-1 monocytes (American Type Tissue Collection) were expanded with non-adherent culture practices in RPMI

media with 10 % heat-inactivated fetal bovine serum in an upright T-25 flask. THP-1 monocytes were differentiated into M0 macrophages with 5 ng/mL phorbol 12-myristate 13-acetate (PMA) for 72 h. A decellularized SIS sheet and electrospun SIS mesh cut to 5 mm discs were secured to a PDMS-coated well plate to enhance macrophage adhesion and contact with the dECM. Macrophages were seeded on the SIS samples at $1x10^5$ per cm^2 and cultured for 72 h at 37 °C. Control macrophages with no dECM exposure were maintained for the same time point. RNA was extracted using a RNeasy Mini Kit following the manufacturer's protocols (Qiagen), and the concentration and purity were evaluated with a NanoDrop OneC (ThermoFisher Scientific). A High-Capacity cDNA Reverse Transcription Kit (ThermoFisher Scientific) was used to perform reverse transcription. RT-qPCR was used to detect the expression of *NOS2, IL12, CD206, IL10, CHI3L1, VEGF, and TGFβ* with a QuantStudio 5 real-time qPCR system (Thermo Fisher Scientific). These gene sets were selected based on their use previously to detect macrophage activation in response to implantable biomaterials [61,62]. The 2ΔΔCt method was used to quantify gene expression with GAPDH as the housekeeping control. The fold change in gene expression was calculated with respect to the control macrophages and the decellularized SIS sheet. Experiments were performed in triplicates, with n > 3 dECM/macrophage biological replicate sets.

3. Results and discussion

Based on our prior work electrospinning suspensions of decellularized skeletal muscle-derived ECM, SIS suspensions were originally prepared from decellularized SIS that was lyophilized, ground into powder, and suspended in HFIP [10,50]. HFIP contains two trifluoromethyl groups that disrupt hydrophobic interactions and a mildly acidic secondary hydroxyl group that can disrupt hydrogen bonds, both of which partially disrupt native ECM structures to allow for SIS suspension and enhance particle interactions that allow for electrospinning [63]. Regardless of concentration or particle size, electrospinning of the SIS suspension was not successful with substantial fiber breakup and beading. The viscosity of the suspensions was between 1 and 4 Pa s, which has previously been shown to be within the electrospinning range of 0.001–50 Pa s [49,64,65]. Increasing the concentration of the suspension to surpass a viscosity of 4 Pa s resulted in swollen particles without a liquid phase that could not be electrospun. Although the viscosity of polymeric electrospinning solutions has been widely used to predict spinnability and fiber morphology [64,66], it was not sufficient to predict the spinnability of these suspensions. Rheological assessment of the SIS suspensions indicated reduced elasticity compared to typical polymeric electrospinning solutions. Chain entanglements in polymer solutions instill elastic properties that resist fiber breakup during the electrostatic drawing of the electrospinning process. We hypothesized that the lack of interaction between distinct particles did not provide sufficient elastic behavior within the suspension to withstand electrostatic drawing. Although the composition of ECM is complex with over 600 proteins, high-level hypotheses can be made about the impact of composition on suspension elasticity. The stiffness of SIS-derived ECM (~14 MPa) is three orders of magnitude higher than the stiffness of skeletal muscle-derived ECM (~40 kPa) indicating stronger intermolecular forces binding the ECM components together [67]. Increased force is required to disrupt strong intermolecular forces and loosen dense ECM particles which could contribute to the lack of interaction between particles and overall elasticity of the suspension. Additionally, SIS-derived ECM contains twice the abundance of non-fibrillar collagens compared to skeletal muscle-derived ECM, which could also reduce the interactions between particles [68]. In order to increase entanglement and elasticity, the SIS suspensions were homogenized prior to electrospinning. A stepwise approach was taken by homogenizing the native form SIS sheet prior to drying and/or homogenizing the SIS suspension immediately prior to electrospinning. In order to develop robust suspension electrospinning methodology, a systematic assessment of key suspension variables was conducted to identify the structural changes within the suspension and the impact on rheological properties that correlated to spinnability.

3.1. Effect of homogenization on particle interaction and fiber formation

First, dilute SIS suspensions were imaged with brightfield microscopy to assess structural changes after homogenization (Fig. 2A). Mixing in HFIP disrupts both hydrophobic interactions and hydrogen bonds, resulting in greater than a 90 % decrease in particle diameter from 500 to 2000 μm in the dry state to around 50 μm in the suspended state. This indicates that the dried particles break down during mixing in HFIP but not to full dissolution. Additionally, the suspensions contained fibrillar components with diameters on the order of microns, similar to the scale of collagen bundles [69]. This indicates protein microstructure was being retained. Homogenization resulted in suspension particles that were less dense and exhibited large fibrillar networks protruding from their core. There was also an increase in free-floating fibrillar content in the suspension. The homogenization of the SIS sheets had a greater impact on the density of the particles and the size of fibrils extending from their core; whereas the homogenization of the suspensions had a greater impact on the concentration of free fibrils in suspension not anchored by a particle. Homogenization of the suspension also led to a 40 % reduction in particle diameter. We hypothesized that these structural changes with homogenization would increase the elasticity of the suspension because the reduced density of the particles, increase in protruding fibrils, and increased fibrillar content would increase particle-particle interaction. To evaluate this hypothesis of particle interaction facilitating elastic behavior, a rheological assessment was conducted.

The relationship between the storage and loss modulus of the suspensions across a range of strain amplitudes was characterized (Fig. 2C and D). In all cases, the suspensions acted as viscoelastic solids at small amplitudes, as noted by the dominance of the storage modulus over the loss modulus, and viscoelastic liquids at large amplitudes, where the loss modulus is larger than the storage modulus. Although the transition from primarily elastic behavior to primarily viscous behavior is complex and transient, the yield point can be estimated from the crossover between the storage and loss modulus. Above the crossover strain, the suspension flows unrecoverably, while below the crossover strain, the suspension undergoes more elastic deformation that can be recovered after the strain is removed. Homogenization of the suspensions had a direct effect on the crossover point. The suspensions that were homogenized had a larger crossover strain amplitude with the homogenization of the SIS sheet having a greater impact than the homogenization of the suspension. The amplitude sweep was conducted in both ascending and descending fashion to determine if the rheological behavior of the suspensions is time-dependent or thixotropic. The suspensions that were homogenized exhibited a larger hysteresis loop indicating increased thixotropic behavior. Similar responses have previously been observed in hydrogels [70]. The homogenization of the SIS sheet had a greater impact on thixotropy than the homogenization of the suspension. Lastly, a flow ramp was conducted to evaluate the rate-dependence of the viscosity of the suspensions (Fig. 2E). Although viscosity alone did not fully predict the spinnability of suspensions, it is an important parameter to assess the full rheological profile of the suspensions. At shear rates greater than 10 s^{-1}, all the suspensions had similar viscosities. Conversely, at shear rates less than 10 s^{-1}, the viscosity increased with increasing homogenization. There was a similar effect observed with both SIS sheet homogenization and suspension homogenization. Collectively, these findings support that homogenization increased the elastic and thixotropic behavior of the SIS suspensions as indicated by increased crossover strain amplitudes and time-dependent responses. We hypothesize that the protruding fibrillar components of the particles in suspension interact and produce drag between particles that is reflected in the increased elasticity of the suspension. When homogenized

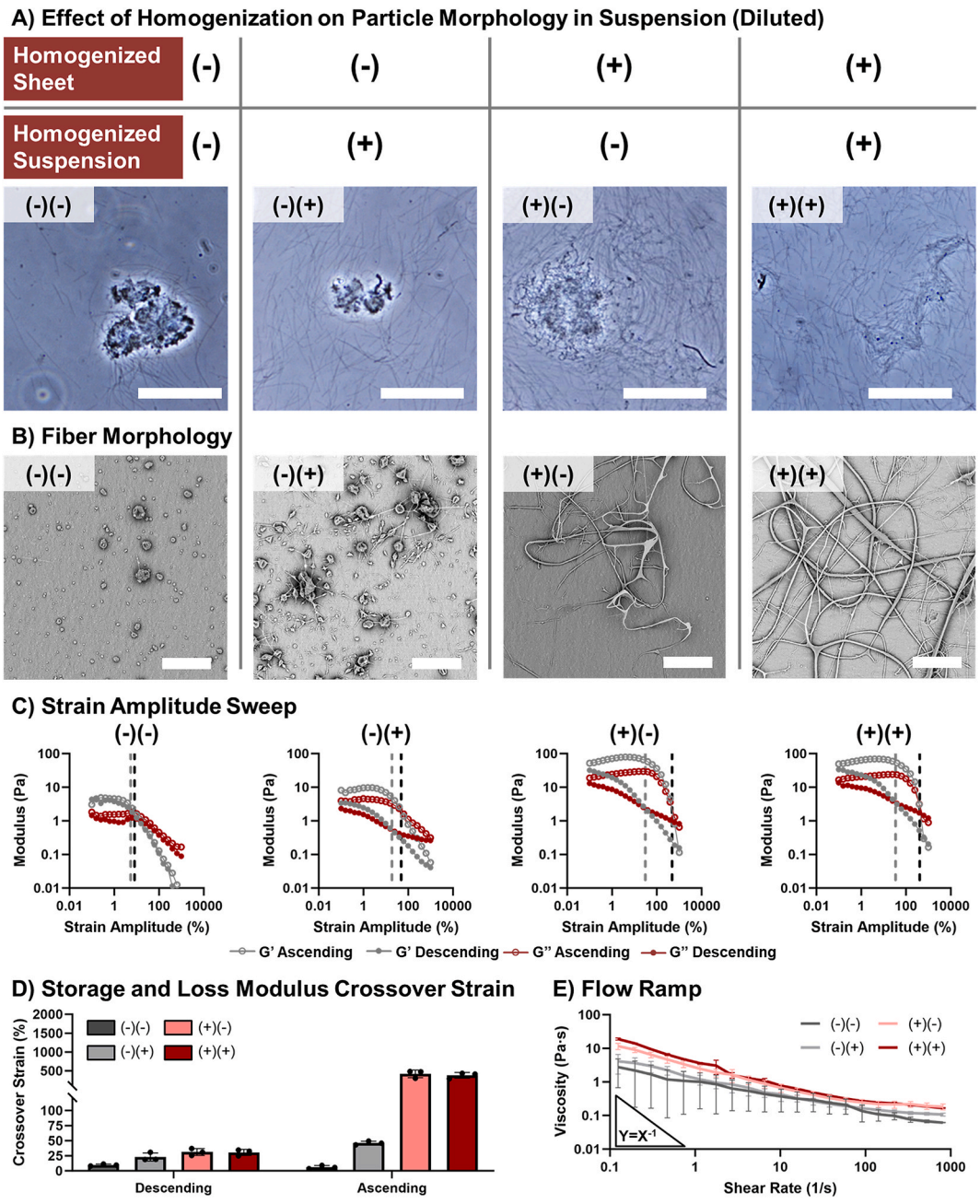

Fig. 2. Effect of homogenization on suspension particle morphology, rheological properties, and fiber collection. A) Brightfield image of dECM particles in an electrospinning suspension. Scale bar = 60 μm. B) SEM images of collection morphology. Scale bar = 20 μm. C) Strain amplitude sweep of dECM suspensions in which solid points were collected with a descending amplitude sweep and hollow points were collected in an ascending manner. The grey dotted line indicates the crossover from the descending amplitude test and the black dotted line indicates the crossover with ascending applied strain. D) The strain amplitude at which the storage and loss moduli cross collected with a descending and ascending strain sweep. E) The rate dependence of the viscosity of the dECM suspensions.

suspensions were tested with an ascending strain amplitude, the interaction of the particles overcomes the applied deformation until a sudden breaking point when the particles separate and the suspension flows. When decreasing the strain amplitude, the particles are initially separated by the large strains and are allowed to slowly establish interactions more gradually. Conversely, the particles within non-homogenized samples can slide past each other similarly regardless of the applied strain history because they lack entanglements. These rheological features were then correlated with the electrospun fiber formation of each processing condition to identify key rheological properties that predict spinnability.

Increased homogenization of the suspensions resulted in a key transition from beads to fibers (Fig. 2B). The homogenization of the SIS sheet had a greater impact than the homogenization of the suspension. The suspensions fabricated from a non-homogenized SIS sheet resulted in a bead-like morphology, and only homogenizing the suspension led to minimal formation of strings branching from the beads. Suspensions from a homogenized SIS sheet resulted in a fibrous morphology, and homogenizing both the sheet and the suspension led to more continuity within the fibers. Based on these results, it was concluded that the crossover strain and level of fibrils protruding from the particles in suspension had a greater impact on spinnability than the free fibrils in suspension. This suggests that the primary mechanism of fiber formation during spinning is the interaction between particles rather than the free fibril network. The fibril network is likely too dilute to withstand the electrostatic forces involved in electrospinning. However, the fibril

network is expected to support the continuity between occasional disparate particles as showcased by broken fibers electrospun with the non-homogenized suspension and continuous fibers electrospun with the homogenized suspension. The ascending strain amplitude at which the dynamic moduli cross was more predictive of fiber formation than the descending crossover point likely because it is more representative of electrospinning-induced strain that increases as the jet travels from the needle to the collector. The crossover strain is a measure of the yield point, at which the suspension behavior changes from being predominantly recoverable, or elastic, to flowing unrecoverably. However, the exact value of the crossover strain does not have a direct equivalence in the spinning process. During electrospinning, the suspensions are drawn into a thin jet and undergo significant strain. The exact strain induced by electrospinning is difficult to quantify but is expected to be between 10^6 – 10^7 s^{-1} [71]. In this context, the crossover strain is interpreted as a measure of elasticity: the larger the crossover strain, the more the structure can be strained recoverably before yielding and flowing. In this manner, it can also be thought of as the strain at which the suspension will break apart into beads during electrospinning. If the applied strain is above the crossover strain amplitude, the suspension will deform viscously and essentially fail [72,73]. Therefore, larger values of the crossover strain represent an enhanced ability to deform elastically before flowing viscously, which in turn is indicative of a more fibrous structure that is favorable for spinning. A direct correlation was observed between this measure of elasticity and the resulting fibrous structure that permitted the definition of a threshold ascending strain amplitude that correlates to spinnability. The suspensions with an ascending crossover strain amplitude of ~400 % resulted in fiber formation; whereas, suspensions with an ascending crossover strain amplitude of <50 % resulted in bead formation. Although the ascending crossover strain amplitude does not fully represent the complex rheological properties that are involved in electrospinning, it is a functional predictor of spinnability.

3.2. Effect of dECM concentration on rheological properties and fiber formation

Using this framework, we next investigated the effects of additional suspension preparation parameters on rheological properties and resulting fiber collection. The impact of solution concentration on electrospun fiber morphology has been extensively reported [49,64,74–78]. Surface tension and the applied electric field overcome the chain entanglements in low-concentration polymeric solutions causing them to break into beads. At higher concentrations, the chain entanglements can withstand electrostatic drawing into a fiber. Suspensions do not follow the same chain entanglement paradigm; rather, it is particle interactions that are the primary mechanism to prevent electrostatic break-up. To characterize the effect of dECM concentration on suspension electrospun fiber morphology, SIS suspensions were prepared with concentrations from 10 to 60 mg/mL. Each suspension was prepared with the Abraham decellularization and preparation technique with a dried particle size of 500–2000 μm and dual homogenization (both the SIS sheet and SIS suspension were homogenized). Suspensions were electrospun and the resulting suspension rheological properties and fiber morphology were characterized (Fig. 3). The ascending crossover strain amplitude of the 10–50 mg/mL suspensions were all similar and greater than 400 % (Fig. 3B and C). This indicates the suspensions are viscoelastic solids and deform elastically at high strains. Interestingly, the 60 mg/mL suspension exhibited a significantly reduced crossover strain amplitude compared to the 10–50 mg/mL suspensions. A flow ramp indicated that the viscosity generally increases with increasing suspension concentration, especially at high shear rates (Fig. 3D). Increasing the concentration of the suspension increases the density of particles and thus, particle interaction. Under shear, increased

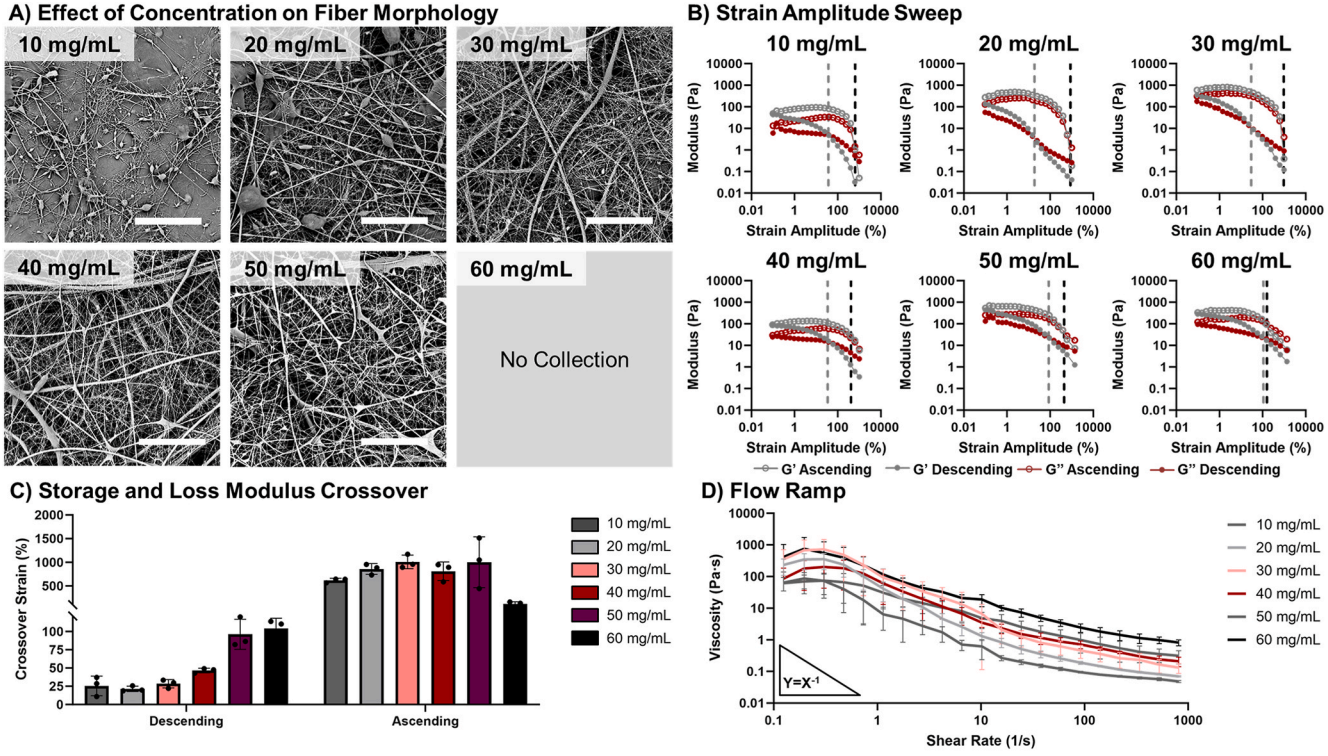

Fig. 3. Effect of SIS concentration on suspension rheological properties and fiber collection. A) SEM images of fiber morphology. Scale bar = 20 μm. B) Strain amplitude sweep of dECM suspensions in which solid points were collected with a descending strain sweep and hollow points were collected with an ascending strain sweep. The grey dotted line indicates the crossover with descending applied strain and the black dotted line indicates the crossover with ascending applied strain. C) The crossover strain of the storage and loss modulus curves collected with descending and ascending strain sweeps. D) dECM suspension viscosity with respect to shear rate.

particle interaction imparts an increased resistance to deformation to the suspension. However, the applied force at which these interactions break remains the same, as seen with the similar crossover strain amplitude required to make the suspension flow. Although the 10–50 mg/mL suspensions resulted in fibrous structures, higher concentrations improved fiber continuity. The 10–20 mg/mL suspensions contained both fibers and beads; whereas, fibers spun from 30 to 50 mg/mL suspensions had continuous fibers without substantial beading (Fig. 3A). Thus, the crossover strain amplitude remains a good predictor of spinnability and fiber formation, but viscosity can be used to improve fiber morphology. The limited particle interaction in low-concentration suspensions is overcome by the electrostatic forces in electrospinning and these suspensions begin to break into beads, as often occurs in dilute polymeric solutions due to limited chain entanglement. Additionally, electrospinning the 10 mg/mL suspension creates a largely fused mesh because the elevated solvent content is unable to sufficiently evaporate before collecting. There was no collection when the 60 mg/mL suspension was electrospun. Voltage was increased up to 30 kV and no Taylor cone was observed. It was hypothesized that the viscosity of the 60 mg/mL suspension was too high for electrostatic drawing even at these higher voltages. Interestingly, the SIS concentration did not significantly impact the fiber diameter distribution of the electrospun mesh (Fig. S1). This is in contrast to polymer solution electrospinning in which increased concentration correlates to increased fiber diameter [77]. Altogether, the observed trends regarding concentration and electrospun fiber morphology of dECM suspensions, except for fiber

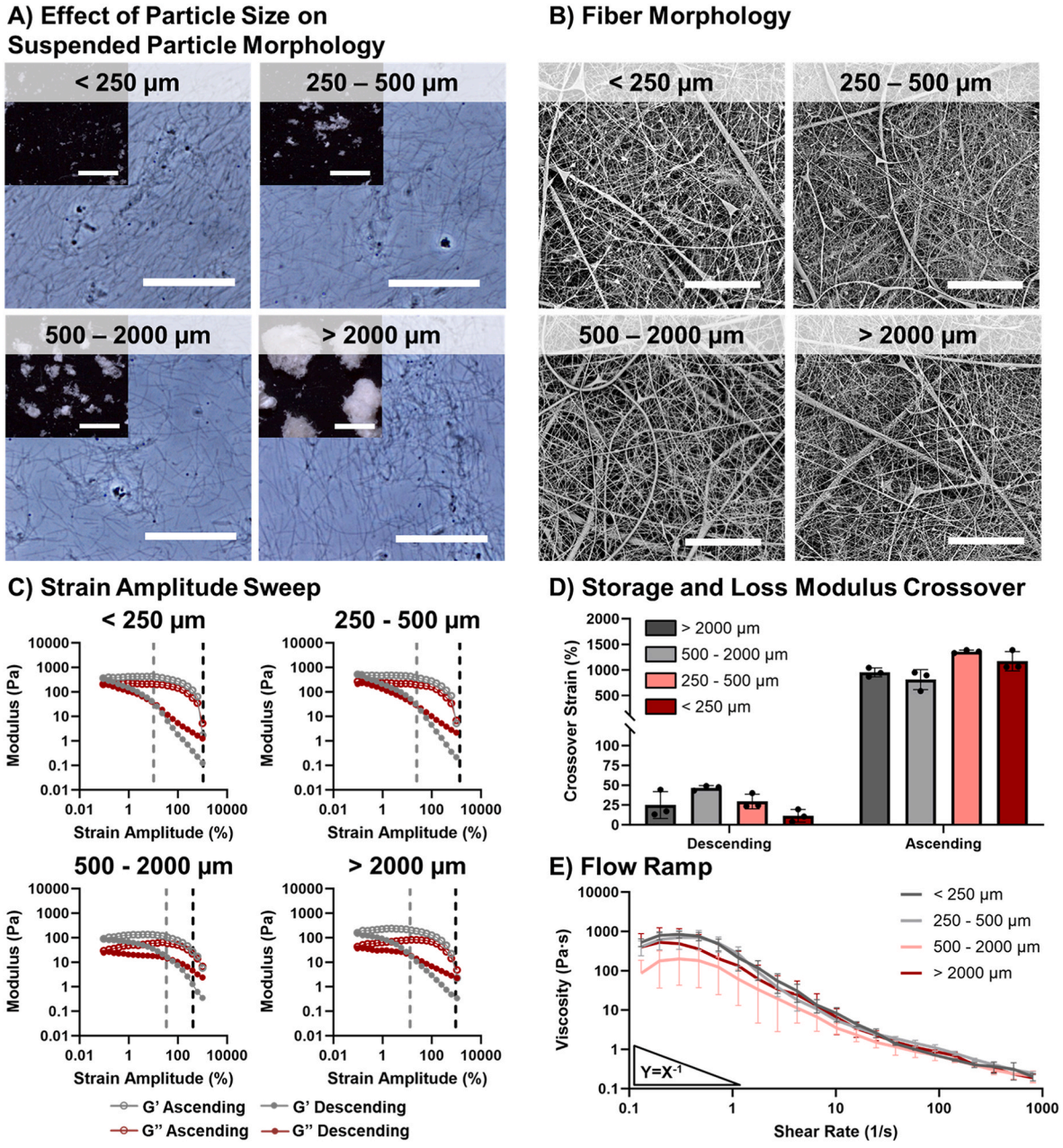

Fig. 4. Effect of dry particle size on suspension particle morphology, rheological properties, and fiber collection. A) Brightfield image of dECM particles in an electrospinning suspension. Scale bar = 60 µm. Inset stereoscope image of dried dECM particles. Scale bar = 3 mm. B) SEM images of fiber morphology. Scale bar = 20 µm. C) Strain amplitude sweep of dECM suspensions in which solid points were collected with a descending strain sweep and hollow points were collected with an ascending strain sweep. The grey dotted line indicates the crossover with descending applied strain and the black dotted line indicates the crossover with ascending applied strain. D) The crossover strain of the storage and loss modulus curves collected with descending and ascending strain sweeps. E) dECM suspension viscosity with respect to shear rate.

diameter, remain consistent with electrospinning polymeric solution literature [49,79]. Thus, the impact of the concentration of particle interaction in suspensions is analogous to chain entanglement in solutions.

3.3. Effect of particle size on rheological properties and fiber formation

Next, we investigated the effect of lyophilized and ground ECM particle size that was suspended in HFIP on suspension electrospinning to determine the level of precision that is required for grinding and filtering tools. The particle size range of ground ECM can vary widely with different grinding techniques, from a scale in nanometers to millimeters. The dual homogenized SIS suspension was prepared with four size ranges of dried SIS particles with an electric blade grinder, including <250 μm, 250–500 μm, 500–2000 μm, and >2000 μm. Each suspension was prepared with the Abraham decellularization and preparation technique and a concentration of 40 mg/mL. Interestingly, the dry particle size from <250 μm to >2000 μm did not significantly impact suspension particle morphology, electrospun fiber morphology, or suspension dynamic moduli (Fig. 4, Fig. S1). Each suspension contained particles on the scale of tens of microns with protruding fibrils and free fibrils similar to the dual homogenized suspension deemed "spinnable" in Fig. 2. These results suggest that the dry SIS particles break down to a consistent equilibrium size and morphology during mixing, regardless of the initial size. Based on this structural analysis, it was not surprising that there was minimal effect of dry particle size on rheological properties or fiber morphology. At low shear rates, there was a small decrease in suspension viscosity with increasing dry particle size, but at high shear rates, there was not a significant effect of particle size. We concluded from these findings that the size of the ground particles does not need to be precisely controlled between 250 and 2000 μm. Thus, expensive tissue grinding methods such as cryo-milling and bead-milling are not required for dECM suspension electrospinning.

Collectively, these studies provide a functional assessment of the critical parameters needed to fabricate dECM meshes using suspension electrospinning. Homogenization is critical to prepare a suspension that deforms elastically under elevated strain amplitudes and can withstand the electrostatic forces in electrospinning (Fig. 2). Instead of chain entanglements that dominate solution electrospinning, dECM suspensions are strongly influenced by inter-particle interactions instilled by loose fibrillar networks protruding from individual particles. Homogenization reduces the density of the particles and increases the fibrillar component within the suspension, which in turn increases the particle interaction and suspension elasticity. Once a spinnable, dual-homogenized suspension was prepared, the impact of concentration and particle size on fiber morphology was evaluated (Figs. 3 and 4). The dECM concentration in the suspension had a similar impact as polymer concentration does in solution electrospinning, with a lower concentration threshold that results in beading and a higher concentration threshold that becomes unspinnable due to resistance to electrostatic drawing. Thus, particle interaction may be considered analogous to chain entanglement with regard to the spinnability of suspensions. In contrast, dry particle size between 250 and 2000 μm did not have a significant impact on suspension properties or electrospun fiber morphology. The dried particles break down to a consistent size and morphology which suggests an equilibrium state of the suspended particles. In addition, preliminary testing indicates that the SIS suspensions are stable for up to 4 days. A stability assessment was conducted by electrospinning SIS suspensions after storage for up to 4 days at 4 °C (Fig. S2). No differences were observed in the electrospinning, fiber collection, or fiber morphology at these time points indicating that the suspensions are not settling or changing significantly over time (Fig. S1). The stability can be attributed to the partially dissolved fibrils entangled with surrounding fibrils and the high concentration of SIS. The stable behavior of the SIS suspensions is similar to the characteristics of colloids and overcomes the traditional limitations of settling in suspensions. Altogether, the input parameters to control electrospun fiber morphology have been characterized with a mechanistic rationale based on particle interaction and elastic rheological behavior. To expand the utility of this methodology, we next examined the effect of the decellularization and preparation techniques and tissue sources on spinnability. Three common SIS decellularization techniques and three tissue sources were used to prepare dECM electrospinning suspensions and the effects on suspension rheology and fiber formation were examined.

3.4. Effect of decellularization and preparation method on fiber formation

SIS-derived ECM is one of the most widely used dECM materials in clinical practice and current research because of its high growth factor content and proven track record for tissue regeneration [1,4]. With its wide use, numerous decellularization and preparation techniques have been established to meet different needs due to the potential impact on dECM composition and bioactivity [52]. Herein, the Abraham [53], Badylak [54,55], and Luo [6,56] decellularization and preparation techniques were investigated to characterize the impact of preparation methodology on SIS suspension properties and spinnability (Fig. 5). The impact of each preparation method on SIS composition has been robustly characterized by Ji et al. [52]. Briefly, the Abraham technique is a strong chemical treatment involving sodium hydroxide and hydrochloric acid. The strong acid and base exposure is effective at removing DNA but can accelerate degradation and remove non-crosslinked collagen. The Badylak technique is a weak chemical treatment with peracetic acid. This method is not as effective at removing DNA but has minimal impact on matrix composition. In contrast to the Abraham and Badylak chemical-only treatment methods, the Luo technique combines an enzymatic treatment of trypsin-EDTA and SDS with a medium chemical treatment of chloroform, methanol, and peracetic acid. The chloroform/methanol treatment is effective for the delipidation of tissues; however, the use of organic solvents can denature globular proteins. Additionally, SDS is a strong detergent that removes glycosaminoglycans and increases susceptibility to collagen denaturation. Overall, stronger treatments are more effective at removing cell components, but they also remove and/or denature ECM components in the process [52]. Thus, the proper preparation method must be chosen based on the application to balance immunogenicity and the preservation of the native ECM for bioactivity retention. Due to the impact of decellularization and preparation on the ECM components, each electrospinning suspension must be tailored for spinnability. Each suspension was prepared with a dried particle size of 500–2000 μm. Viscosity ranges were determined from the previous study to guide suspension preparation that would be spinnable and limit beading. The Abraham suspension was prepared with a concentration of 40 mg/mL, the Badylak suspension was prepared with a concentration of 60 mg/mL, and the Luo suspension was prepared with a concentration of 70 mg/mL. The varied concentration required to prevent beading may be due to the level of intermolecular forces within the ECM retained after the decellularization and preparation treatment. According to Ji et al., Abraham, Badylak, and Luo SIS retain 717, 644, and 135 different types of proteins, respectively, which inversely correlates to the SIS concentration required to prevent beading [52]. Electrospun meshes were successfully fabricated from all three of the decellularization and preparation techniques tested, but the suspension properties and electrospun fiber morphology from the Luo technique differed from the Abraham and Badylak techniques (Fig. 5). The Abraham and Badylak techniques show more similar particle morphology with similar size and fibril protrusions; whereas, the Badylak suspension had more dense particle cores (Fig. 5A). This was attributed to the reduced chemical treatment maintaining stronger protein-protein interactions that are more difficult to disrupt with homogenization. The Luo suspensions contain larger conglomerates of suspended fibrils on the order of 100 μm. The Luo dECM is likely more homogenous due to increased digestion and processing; whereas, the Abraham and Badylak suspension particles likely

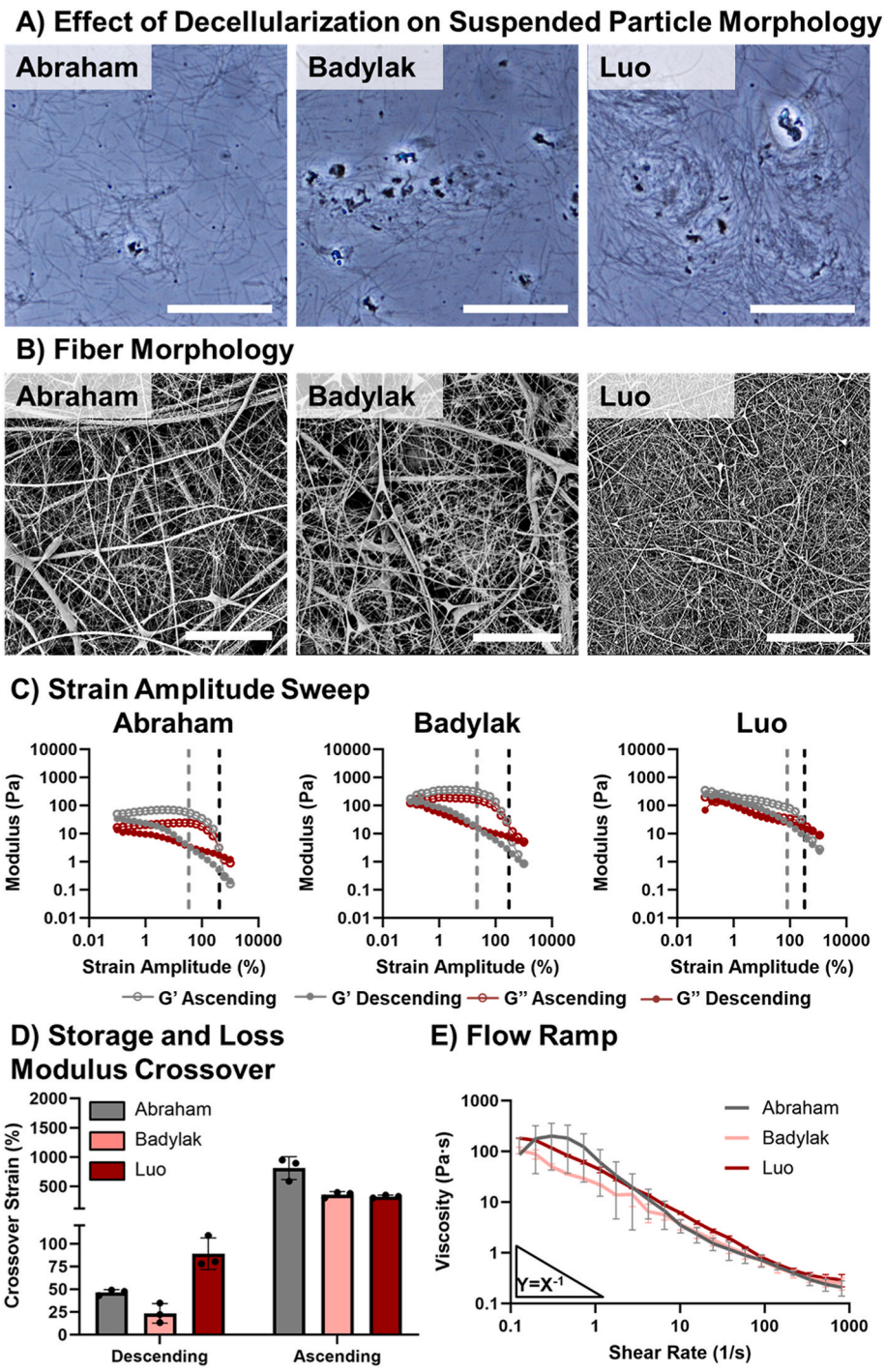

Fig. 5. Effect of SIS decellularization and preparation method (Badylak, Abraham, and Luo) on suspension particle morphology, rheological properties, and fiber collection. A) Brightfield image of dECM particles in an electrospinning suspension. Scale bar = 60 μm. B) SEM images of the electrospun dECM fibers. Scale bar = 20 μm. C) Strain amplitude sweep of dECM suspensions in which solid points were collected with a descending strain sweep and hollow points were collected with an ascending strain sweep. The grey dotted line indicates the crossover with descending applied strain and the black dotted line indicates the crossover with ascending applied strain. D) The crossover strain of the storage and loss modulus curves collected with a descending and ascending strain sweep. E) dECM suspension viscosity with respect to shear rate.

break along areas of weaker protein binding innate to a heterogeneous mixture of ECM components. In terms of rheology, the ascending crossover strain amplitude remained consistent across techniques indicating that their ability to resist flowing and breaking under electrostatic forces is similar (Fig. 5D). This is supported by the continuous fiber formation seen in each electrospun mesh (Fig. 5B). However, the raw dynamic moduli curves with respect to strain amplitude differed (Fig. 5C). Although the loss and storage modulus crossover strain amplitude were the same, the negative slope of the dynamic moduli at low strain amplitudes was unique to the Luo suspension. The Abraham and Badylak suspensions exhibited a plateau in the dynamic moduli at low strain amplitudes. This suggests that the particles in the Luo suspension were continuously deforming as strain amplitude increased until the particle interactions were overcome, and the suspension began to flow. In contrast, the particles in the Abraham and Badylak suspensions were expected to remain static and hold together more consistently

until a threshold was reached to separate the particles and initiate flow of the suspension. It was hypothesized that the enzymatic treatment in the Luo technique disrupts protein interaction via denaturation and reduces the binding or attraction force between the particles in suspension. This allowed the particles to deform with greater ease under applied strain. When electrospinning, the Luo suspensions can deform gradually and more homogenously to form fibers with a reduced diameter and more narrow fiber distribution (Fig. S1). The proteins can rearrange more easily under applied strain without completely breaking apart due to the weaker protein interaction and bigger particle conglomerates. These results further support the use of the ascending crossover strain amplitude as a predictor of spinnability. Although the Luo suspension has complex rheological properties that impact fiber morphology differently compared to the Abraham and Badylak suspensions, the spinnability and fiber formation remain consistent. Additionally, the more narrow fiber diameter distribution within the mesh electrospun from the Luo suspension further reinforces the idea that increased digestion of dECM is beneficial to homogenous processing and mesh fabrication. However, it is well established that enzymatic digestion denatures proteins and reduces the bioactivity of dECM [24]. It is expected that increased homogenization and processing of the Abraham- and Badylak-derived ECM could similarly reduce the fiber diameter distribution of the meshes. However, excess heat from prolonged homogenization or enzymatic treatment would increase the risk of altering the bioactivity of the ECM via denaturation. Considering that the same tissue source and electrospinning parameters resulted in varied fiber morphology shows that decellularization method plays a direct role in electrospinning characteristics and final mesh architecture. Therefore, researchers must recognize the interplay between mesh morphology and denaturation and balance the need for homogenous fiber structures with the retention of bioactivity.

3.5. *Effect of tissue source on fiber formation*

The bioactivity of dECM scaffolds is strongly dependent on the tissue source of the dECM. Each tissue has a specialized set of proteins, proteoglycans, and growth factors that are tailored to the functions of the tissue [68]. For example, SIS and dermal tissues contain a high concentration of growth factors, such as VEGF, TGFβ, and bFGF, to support a high level of tissue remodeling. Alternatively, cardiac tissue contains an

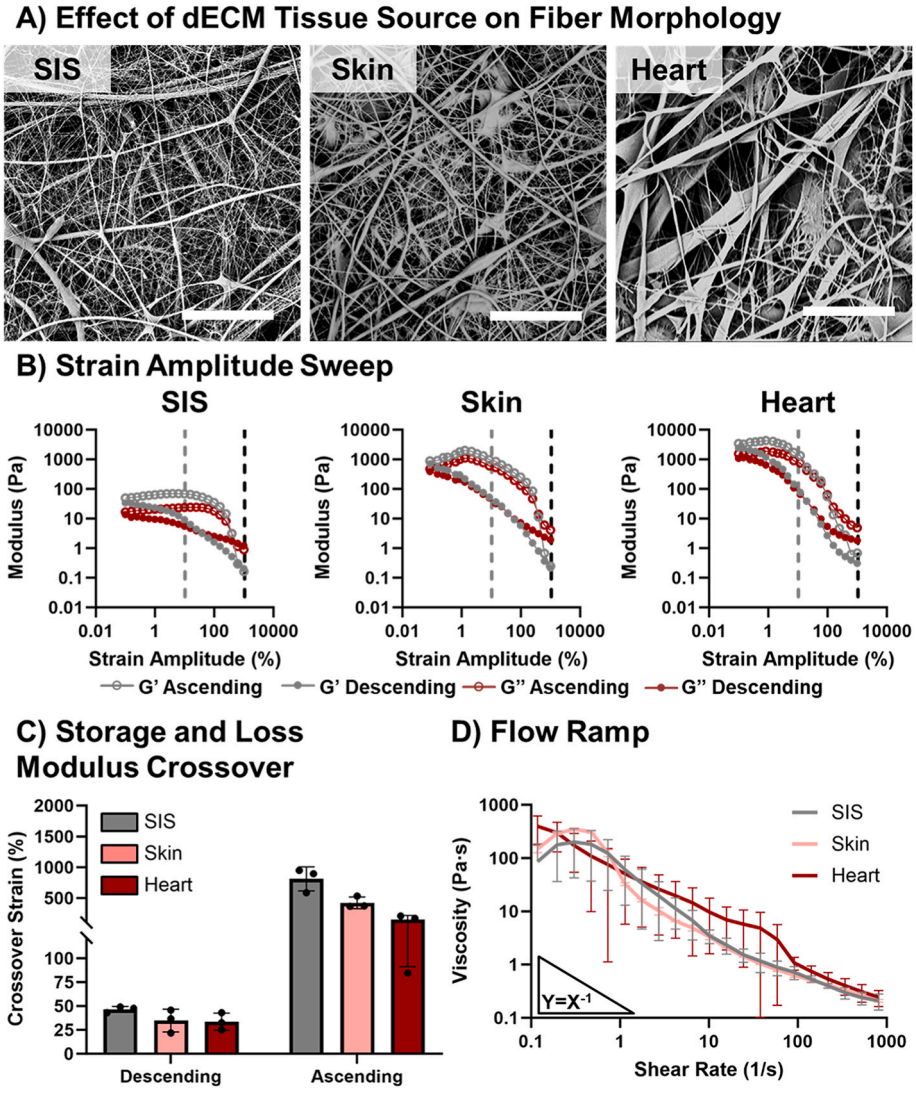

Fig. 6. Effect of tissue source (SIS, skin, heart) on suspension particle morphology, rheological properties, and fiber collection. A) SEM images of the electrospun dECM fibers. Scale bar = 20 μm. B) Strain amplitude sweep of dECM suspensions in which solid points were collected with a descending strain sweep and hollow points were collected with an ascending strain sweep. The grey dotted line indicates the crossover with descending applied strain and the black dotted line indicates the crossover with ascending applied strain. C) The crossover strain and modulus of the storage and loss modulus curves collected with a descending and ascending strain sweep. D) The viscosity with respect to the shear rate of the dECM suspensions.

abundance of fibronectin to maintain homeostasis and recruit myofibroblasts for repair [4,68,80,81]. Tissue engineering scaffolds used to treat various tissues and diseases may require a broad range of dECM tissue sources. Thus, the established suspension electrospinning must be functional with many types of dECM. In this study, dECM suspensions were prepared from SIS, skin, and cardiac tissues (Fig. 6). Each suspension was prepared with a dried particle size of 500–2000 μm. For adequate decellularization efficiency, the SIS- and skin-derived ECM were prepared with the Abraham technique, and the heart tissue was prepared with the Badylak technique. To ensure the suspensions had a viscosity that prevented beading, the SIS suspension was prepared with a concentration of 40 mg/mL, the skin suspension was prepared with a concentration of 70 mg/mL, and the Luo suspension was prepared with a concentration of 55 mg/mL. The viscosity flow ramps of the suspensions composed with each dECM tissue source were similar. The ascending crossover strain amplitude of the SIS and skin suspensions were also similar (~400 %); whereas, the heart suspension had an ascending crossover strain amplitude that was significantly lower (~150 %) (Fig. 6C). This indicates that there was reduced particle interaction in the cardiac suspension. Given that these suspensions were all prepared with dual homogenization, these differences were attributed to the specific composition of the cardiac dECM that reduces the particle interaction forces within the suspension. The complex makeup of ECM, including over 600 proteins, makes it difficult to pinpoint specific components that are impacting the overall rheological properties of the ECM composition. Briefly, cardiac-derived ECM has a lower collagen content than intestine- and skin-derived ECM, of which the cardiac-derived ECM contains a higher percentage of non-fibrillar collagen [68]. Fibrillar collagen can form fibril protrusions from the suspended particles and could contribute to the bulk elasticity of the suspension. Additionally, cardiac-derived ECM has been reported to have less fibrillin-2 than intestine- and skin-derived ECM [68]. Fibrillin-2 contributes to the elasticity of tissues allowing them to stretch. In suspension, the presence of fibrillin-2 could contribute to the elevated crossover strain amplitude which facilitates electrospinning. Once electrospun, a mesh composed of continuous fibers was fabricated with each dECM tissue source indicating that a crossover strain amplitude of 150 % is sufficient to maintain elasticity and withstand the electrostatic drawing involved in electrospinning. This further refines the acceptable range of suspension properties for spinnability, where <50 % crossover strain amplitude is primarily beads and >100 % forms continuous fibers when electrospun. Although these suspensions were all spinnable, the fiber morphology differed. The mesh composed of skin-derived ECM contained localized areas of fusion and webbing, and the mesh composed of heart-derived ECM contained flat ribbon-like fibers with a larger fiber diameter than the fibers in the SIS- and skin-based meshes (Fig. S1). Skin tissue has localized areas of hydrophobic and hydrophilic domains to provide a sufficient external barrier and prevent infection [82,83]. The varying compositions may phase separate during homogenization and mixing and cause localized areas of altered fiber morphology. For the cardiac-derived ECM mesh, ribbon formation has been previously attributed to reduced drying of the solvent leading to fiber collapse and the reduced stretching or elasticity of the solution during drawing [49]. Since each suspension contains the same solvent and spinning conditions, it is unlikely that the evaporation rate of HFIP during electrospinning was different between the SIS-, skin-, and heart-derived ECM suspensions. However, the reduced crossover strain amplitude of the heart dECM suspension indicates a reduction of elasticity of the suspension at higher strains. Thus, the suspension was drawn less under electrostatic forces resulting in bigger fibers that dried quickly on the outside and collapsed before the inner fiber could completely dry and retain its shape.

These studies demonstrate the versatility and robustness of the dECM suspension electrospinning technique. The rheological framework that we have developed provides mechanistic explanations for differences in electrospun fiber morphology and can be used to rationally design the suspension preparation to balance design requirements. Enzymatic treatment can be used to create more homogenous fibrous meshes but risks a reduction in the bioactivity of the mesh via denaturation. Additionally, these initial studies indicate that the dECM tissue source will likely impact the suspension rheological properties and fiber morphology of the electrospun mesh based on different compositions, but spinnable suspensions have a consistent ascending crossover strain amplitude above 100 %. To prepare ECM suspensions from different compositions, an ascending crossover strain above 100 % was targeted with the implementation of homogenization. Afterward, concentration was tuned to achieve a suspension viscosity that supports fiber formation without beading, in this case between 3 and 6 Pa s. The concentration required to prevent beading varied between compositions due to varying intermolecular forces and surface tension. A table comparing the preparation parameters of each suspension composition is included in Supplemental Information to provide guidance on how to prepare spinnable suspensions from a new composition (Table S1).

3.6. *Effect of electrospinning on the biochemical characterization of dECM*

Given that the dECM suspensions retained protein microstructure above the tertiary organization level, as indicated by fibrillar components on the same scale as collagen bundles, it was hypothesized that the electrospun dECM meshes would retain the bioactivity of native dECM. To test this hypothesis, we next examined the biochemical composition and biological activity of the SIS dECM before and after electrospinning. The following biological characterization was conducted on native SIS isolated from porcine small intestine washed in PBS (native SIS), SIS decellularized and prepared with the Abraham technique (decellularized SIS), and a mesh electrospun from SIS also decellularized and prepared with the Abraham technique (electrospun SIS) to isolate the impact of electrospinning from SIS preparation. Each protein has a specific conformation, or 3-dimensional structure, that dictates its biological function. This conformation is the thermodynamically stable form of the specific amino acid sequence that composes the protein and environmental conditions [84]. Protein denaturation, the unfolding of proteins due to the disruption of intermolecular bonds, in response to processing conditions such as heat, detergents, and chemical reagents [85–87] can change cell and enzyme binding site presentation. Denatured proteins lose their bioactivity, or native biological function, and are more readily digested by proteolytic enzymes [88]. Because denaturation is an endothermic process, DSC was conducted to evaluate the impact of the suspension electrospinning processing conditions on the SIS thermal denaturation profile (Fig. 7A). Native SIS, decellularized SIS, and electrospun SIS were compared to isolate the impact of decellularization and electrospinning. Each SIS group exhibited a similar thermal denaturation profile, as indicated by statistically similar ($p > 0.05$) onset temperature, peak temperature, and enthalpy of denaturation. In contrast, when native SIS is partially denatured with a 70 °C heat treatment, the onset temperature, peak temperature, and enthalpy of denaturation are increased. Full denaturation of the native SIS was observed after a full heating ramp to 200 °C, as indicated by complete loss of the denaturation peak in the second cycle (Fig. S1). This indicates that DSC thermograms can characterize the impact of processing on denaturation by measuring the endothermic protein unfolding and loss of intermolecular bonding. Because the thermal denaturation peaks of the three SIS groups (native SIS, decellularized SIS, electrospun SIS) were similar, it was concluded that neither the Abraham preparation process nor the suspension electrospinning process significantly denatured the SIS.

In addition to denaturation, the total protein, collagen, and sulfated glycosaminoglycan (sGAG) content of the native, decellularized, and electrospun SIS were evaluated. Proteins are primarily responsible for the mechanical integrity and structure of ECM. Specifically, collagen is the most abundant protein in ECM that regulates tensile strength, cell

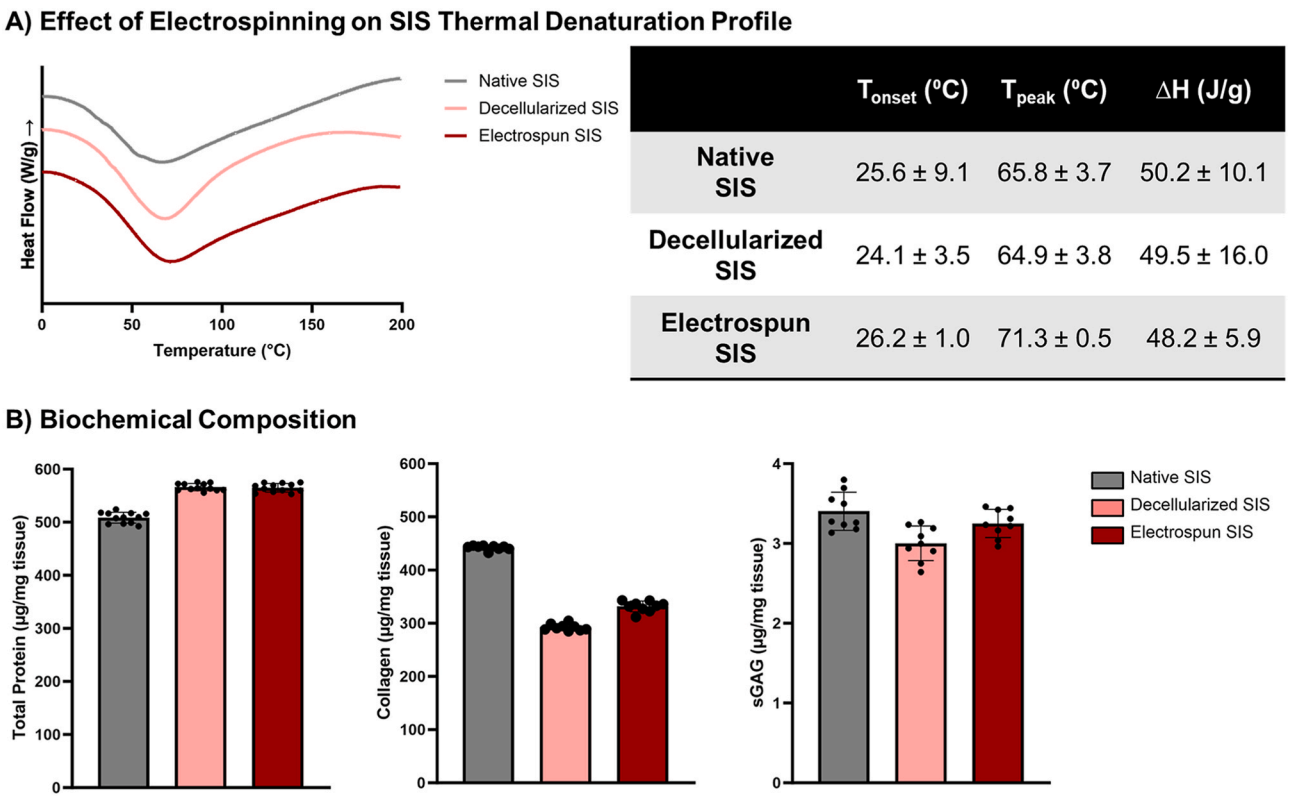

	T_{onset} (°C)	T_{peak} (°C)	ΔH (J/g)
Native SIS	25.6 ± 9.1	65.8 ± 3.7	50.2 ± 10.1
Decellularized SIS	24.1 ± 3.5	64.9 ± 3.8	49.5 ± 16.0
Electrospun SIS	26.2 ± 1.0	71.3 ± 0.5	48.2 ± 5.9

Fig. 7. The effect of electrospinning on SIS composition. A) Differential scanning calorimetry thermogram with the onset temperature, peak temperature, and enthalpy of denaturation. B) Biochemical composition of SIS including total protein, collagen, and sGAG content.

adhesion, and chemotaxis among many other characteristics [89]. Lastly, sGAGs including heparin sulfate and chondroitin sulfate, sequester growth factors, modify cell hydration, and mediate cell signaling [90]. The total protein content per mg tissue within the decellularized and electrospun SIS was elevated compared to the native SIS, which was attributed to the loss of cell mass during SIS decellularization and preparation. As expected, the total protein content was similar between the decellularized and electrospun SIS. The collagen composition was reduced in the decellularized SIS compared to the native SIS. Strong acids and bases disrupt the hydrogen bonds within dECM, which may have resulted in partial solubilization and removal of collagen content during decellularization and preparation. In contrast, the collagen content was increased by 13 % in the electrospun SIS compared to the decellularized SIS. This could be due to the digestion impacting the assay. The decellularized SIS is thicker with a lower surface area, so the presentation of hydroxyproline may be reduced. The sGAG content was similar between the native, decellularized, and electrospun SIS, indicating that neither the SIS decellularization and preparation process nor the electrospinning process significantly impacted the percent sGAG composition in the SIS. Although no large changes were seen after electrospinning, these assays do not completely represent the complex compositional makeup of SIS. In the future, proteomics, involving tissue-specific proteins, could provide a more comprehensive review of the impact of electrospinning on SIS composition and denaturation. However, parsing out the biological impacts of each compositional change will take extensive study. To evaluate the functional impact of electrospinning on SIS bioactivity efficiently, *in vitro* and *in ovo* biological assays assessing cell proliferation, angiogenesis, and immunomodulatory properties were conducted.

3.7. Bioactivity retention of electrospun dECM

As an initial assessment of cytocompatibility, cell attachment and proliferation were evaluated by culturing human dermal fibroblasts on electrospun SIS meshes, and the metabolic activity of the cells was measured using an MTS assay after 1, 3, and 7 days. The metabolic activity of the cells cultured on each substrate increased over time with no significant difference between the electrospun SIS mesh and the decellularized SIS sheet that had no contact with HFIP (Fig. S4). This indicated that the suspension in HFIP and the electrospinning process did not have a negative impact on cell attachment and proliferation to the SIS substrate. Additionally, these results highlight the capacity of electrospun ECM meshes to support cell growth and tissue formation and indicate their potential use as tissue scaffolds. Considering that ECM meshes were fabricated from a variety of tissue sources, the suspension electrospinning platform has the potential to fabricate ECM scaffolds from tissue sources that have been relegated to powders thus far and mimic the native ECM composition of a target organ system.

The angiogenic capacity of SIS has been widely studied and is one of the primary considerations when selecting SIS as a regenerative scaffold material [5,6,91–93]. An *in vitro* tube formation study and an *in ovo* chorioallantoic membrane (CAM) assay were both conducted to robustly assess the impact of electrospinning on SIS angiogenic bioactivity. For the tube formation study, HUVECs were cultured on Reduced Growth Factor Matrigel® in SIS-conditioned media for 4 h (Fig. 8A). The number of capillary-like networks formed in response to the conditioned media was compared between a blank control, a positive VEGF control (20 ng/mL), a decellularized SIS sheet, and an electrospun SIS mesh. All media groups supported some level of tube formation due to the angiogenic cues in Matrigel. However, the increase in networks that formed in response to the positive VEGF control compared to the negative blank control indicated that the network-forming capacity of the HUVECs was not saturated. Further, both SIS substrates supported elevated network formation compared to the blank control and are similar to the VEGF control. Also, the electrospun SIS-conditioned media supported similar network formation to the decellularized SIS

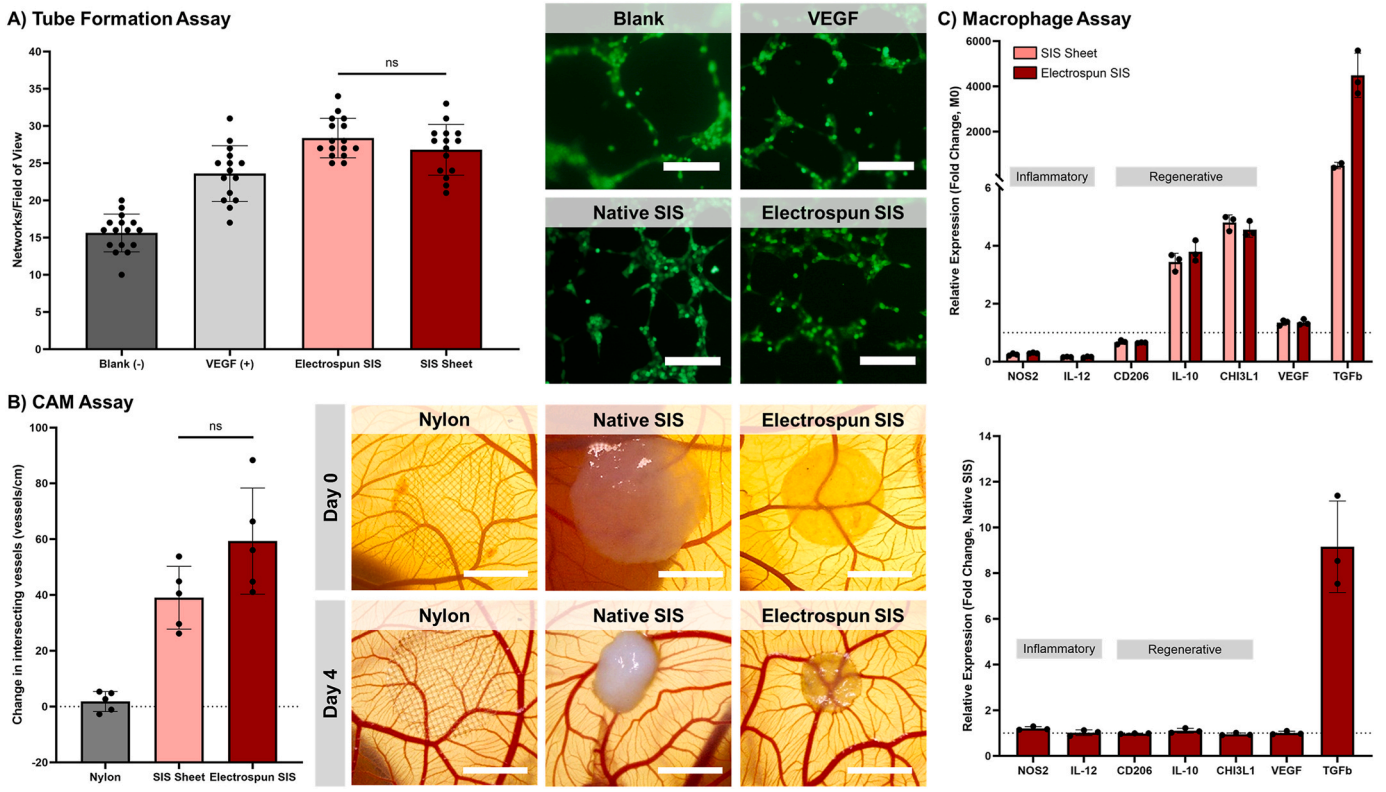

Fig. 8. Evaluation of bioactivity retention after electrospinning. A) *In vitro* HUVEC tube formation in SIS-conditioned media. Scale bar = 500 μm. B) *In ovo* vascularization in a CAM assay after 4 days of sample placement. Vessel density is calculated as the change in the number of vessels intersecting with the sample from Day 0 to Day 4, normalized to the sample perimeter. Scale bar = 3 mm. C) Macrophage gene expression after 72 h of SIS contact with respect to the expression of the M0 control (top) and native SIS (bottom).

sheet-conditioned media. This indicates that the electrospinning process did not negatively impact the angiogenic capacity of the SIS with regard to release products. Since the tube formation assay is limited to the assessment of release products and is artificially inflated by the Matrigel, a CAM assay was conducted for a more robust analysis of the SIS angiogenic capacity. After 10 days of quail embryo culture, a nylon mesh (negative control) [94], decellularized SIS sheet, and electrospun SIS mesh were placed on the CAM for an additional 4 days (Fig. 8B). The change in vasculature was assessed over time with daily imaging. After 4 days of treatment, the primary change in vasculature expected to be seen is small capillary-like vessels, so the vessel density was quantified as the number of vessels intersecting the sample perimeter instead of a vessel area calculation that is heavily skewed by large vessels and sample placement. The Nylon mesh negative control did not significantly impact the vessel density after 4 days on the CAM, indicating that angiogenic cues are needed to increase the vasculature within this timeframe and merely agitation or sample placement on the membrane does not impact angiogenesis. Both of the SIS substrates supported elevated vessel formation compared to the Nylon mesh, and the electrospun SIS mesh supported similar levels of vessel formation compared to the decellularized SIS sheet. Both of the SIS substrates also reduced in size after 4 days on the CAM meaning cells likely migrated into the samples and contracted the ECM. Together, the tube formation assay and CAM assay supported that the angiogenic capacity of the SIS was retained and not negatively impacted after being electrospun.

Lastly, the immunomodulatory bioactivity of the electrospun SIS was evaluated via a macrophage polarization assay. The macrophage response to a material has been used to assess whether a material will elicit pro-inflammatory versus regenerative host response [95,96]. For this reason, THP-1-derived macrophages were cultured on the decellularized SIS sheet, electrospun SIS mesh, and a PDMS control. Fold change in gene expression of the macrophages after 72 h of exposure to dECM was quantified in the following genes: *NOS2, IL12, CD206, IL10, CHI3L1, VEGF,* and *TGFβ* (Fig. 8C). The SIS substrates induced a reduction in inflammatory *NOS2* and *IL12* gene expression and increased gene expression of *IL10, CHI3L1,* and *TGFβ* compared to the M0 naive control. This indicated that SIS substrates drove macrophages toward tolerogenic polarization. The expression of macrophages cultured on the electrospun SIS mesh was largely similar to the decellularized SIS sheet, with statistically similar ($p > 0.05$) expression of *NOS2, IL12, CD206, IL10, CHI3L1*, and *VEGF*. The only gene impacted differentially by the electrospun mesh was *TGFβ,* where there was a 10-fold increase in *TGFβ* expression between the electrospun SIS mesh and the decellularized SIS sheet. Physical characteristics of the electrospun wrap, including the random fiber morphology, are known to alter macrophage activation and could be a potential driving factor in this differential gene expression response [97,98]. *TGFβ* plays a role in tissue remodeling by supporting tissue regeneration without scar formation and increasing expression of *IL10* and *CD206* in macrophages [99,100]. Electrospinning did not largely impact the immunoregulatory bioactivity of SIS via macrophage gene expression with the exception of *TGFβ* and supports a tolerogenic and anti-inflammatory immune response at the time point evaluated. Classically pro-inflammatory genes were not induced suggesting that these electrospinning methods do not fundamentally alter the macrophage response to SIS nor is there residual solvent that induce a stress or damage response. Collectively, the angiogenic and immunomodulatory bioactivity of SIS was not significantly impacted by suspension electrospinning. This is largely attributed to the lack of enzymatic digestion and additives required in processing and the retention of protein microstructure above the tertiary organization level.

Collectively, these findings outline the critical suspension parameters required to electrospin ECM without digestion or additives for diverse tissue engineering applications. Although promising, the

bioactivity assessment in this work was limited to an *in vitro* setting. Evaluation of the cytocompatibility, angiogenesis, and immunoregulation of the electrospun ECM mesh in a subcutaneous rat model is currently under investigation. In addition to bioactivity retention assessments, the impact of processing and electrospinning on mesh resorption rate will be determined. Additionally, the use of HFIP in this ECM electrospinning system limits the scale-up and clinical translation of ECM scaffolds due to the associated environmental hazards and health risks. Recent work on electrospinning natural polymers with biologically benign solvents like acetic acid and a 20X PBS/ethanol mixture suggests that ECM electrospinning could transition to a green solvent system in the future [101,102].

4. Conclusion

In this study, we conducted a rigorous evaluation of dECM suspension properties necessary to support fiber formation during electrospinning. Homogenization was used as a mechanism to increase particle interaction and elastic behavior of the dECM suspensions. The crossover strain amplitude of the loss and storage modulus curves above 100 % was identified as a functional rheological predictor of a spinnable dECM suspension. The sensitivity of fiber morphology to suspension concentration was similar to polymer solution concentration trends in electrospinning. Interestingly, fiber morphology and spinning were relatively independent of the dried particle size as the suspended particles broke down to a consistent state. The versatility of this dECM suspension electrospinning approach was showcased by utilizing three different decellularization and preparation techniques and three different dECM tissue sources with varying compositions which indicates the potential to fabricate ECM scaffolds from tissue sources that have been relegated to powders thus far and mimic the native ECM composition of a target organ system. These groups displayed similar rheological predictors of spinnability; namely, a crossover strain amplitude above 100 %. These studies illustrate the impact of each of the dECM preparation steps on fiber collection so that the protocol can be readily adapted for a specific tissue source and application. Our primary goal in developing this new suspension electrospinning method was to increase bioactivity retention of the mesh after processing, which is a primary limitation of current dECM spinning methods that use synthetic polymer blends or enzymatic digestion. The regenerative capacity of these electrospun SIS meshes was shown to be similar to the decellularized SIS sheet controls with regard to cell proliferation, angiogenesis, and immunomodulation. Overall, this study elucidated the critical parameters that guide dECM suspension electrospinning to provide researchers with a framework to use this new approach to create dECM scaffolds that retain their native regenerative capacity.

Conflicts of interest

There are no conflicts of interest to disclose.

Ethics approval and consent to participate

The authors declare that there are no human or animal subjects used in this research paper. Therefore, no IRB or ethical committee approvals were required.

CRediT authorship contribution statement

Sarah Jones: Writing – original draft, Visualization, Methodology, Investigation, Formal analysis, Data curation, Conceptualization. **Sabrina VandenHeuvel:** Methodology, Formal analysis, Data curation. **Andres Luengo Martinez:** Methodology, Data curation. **Ruchi Birur:** Methodology, Data curation. **Eric Burgeson:** Methodology. **Isabelle Gilbert:** Data curation. **Aaron Baker:** Supervision, Methodology, Formal analysis. **Matthew Wolf:** Writing – review & editing. **Shreya A. Raghavan:** Writing – review & editing, Supervision, Methodology, Investigation, Formal analysis. **Simon Rogers:** Writing – review & editing, Supervision, Formal analysis. **Elizabeth Cosgriff-Hernandez:** Writing – review & editing, Visualization, Supervision, Resources, Project administration, Methodology, Investigation, Funding acquisition, Formal analysis, Conceptualization.

Declaration of competing interest

The authors declare that they have no known competing financial interests or personal relationships that could have appeared to influence the work reported in this paper.

Acknowledgments

Funding for this work was supported by the National Science Foundation Graduate Research Fellowship Program under Grant (award # 2020300397). Any opinions, findings, conclusions, or recommendations expressed in this material are those of the author(s) and do not necessarily reflect the views of the National Science Foundation.

Appendix A. Supplementary data

Supplementary data to this article can be found online at https://doi.org/10.1016/j.bioactmat.2024.08.012.

References

[1] S.F. Badylak, The extracellular matrix as a biologic scaffold material, Biomaterials 28 (25) (2007/09/01/2007) 3587–3593.
[2] L. Huleihel, et al., Matrix-bound nanovesicles within ECM bioscaffolds, Sci. Adv. 2 (6) (2016) e1600502.
[3] T.A. Wilgus, Growth factor-extracellular matrix interactions regulate wound repair, Adv. Wound Care 1 (6) (Dec 2012) 249–254 (in eng).
[4] S.F. Badylak, D.O. Freytes, T.W. Gilbert, Extracellular matrix as a biological scaffold material: structure and function, Acta Biomater. 5 (1) (2009/01/01/2009) 1–13.
[5] F. Li, W. Li, S. Johnson, D. Ingram, M. Yoder, S. Badylak, Low-molecular-weight peptides derived from extracellular matrix as chemoattractants for primary endothelial cells, Endothelium 11 (3–4) (May-Aug 2004) 199–206 (in eng).
[6] W. Wang, et al., Preparation and characterization of pro-angiogenic gel derived from small intestinal submucosa, Acta Biomater. 29 (2016/01/01/2016) 135–148.
[7] S.F. Badylak, J.E. Valentin, A.K. Ravindra, G.P. McCabe, A.M. Stewart-Akers, Macrophage phenotype as a determinant of biologic scaffold remodeling, Tissue Eng. 14 (11) (2008) 1835–1842.
[8] B.M. Sicari, J.L. Dziki, B.F. Siu, C.J. Medberry, C.L. Dearth, S.F. Badylak, The promotion of a constructive macrophage phenotype by solubilized extracellular matrix, Biomaterials 35 (30) (2014) 8605–8612.
[9] J.E. Valentin, A.M. Stewart-Akers, T.W. Gilbert, S.F. Badylak, Macrophage participation in the degradation and remodeling of extracellular matrix scaffolds, Part. Accel. 15 (7) (2009) 1687–1694 (in eng), *Tissue engineering*.
[10] M.M. Smoak, K.J. Hogan, K.J. Grande-Allen, A.G. Mikos, Bioinspired electrospun dECM scaffolds guide cell growth and control the formation of myotubes, Sci. Adv. 7 (20) (2021) eabg4123.
[11] Y. Wu, et al., Implantation of brain-derived extracellular matrix enhances neurological recovery after traumatic brain injury, Cell Transplant. 26 (7) (Jul 2017) 1224–1234 (in eng).
[12] R. Mazloomnejad, et al., Angiogenesis and Re-endothelialization in decellularized scaffolds: recent advances and current challenges in tissue engineering, Front. Bioeng. Biotechnol. 11 (2023-February-16 2023) (in English).
[13] J.V. Nayak, et al., Porcine small intestine submucosal grafts improve remucosalization and progenitor cell recruitment to sites of upper airway tissue remodeling, International Forum of Allergy & Rhinology 8 (10) (2018/10/01 2018) 1162–1168, https://doi.org/10.1002/alr.22156.
[14] W.S. Helton, P.M. Fisichella, R. Berger, S. Horgan, N.J. Espat, H. Abcarian, Short-term outcomes with small intestinal submucosa for ventral abdominal hernia, Arch. Surg. 140 (6) (Jun 2005) 549–560, discussion 560-2(in eng).
[15] L. Ansaloni, et al., Immune response to small intestinal submucosa (surgisis) implant in humans: preliminary observations, J. Invest. Surg. 20 (4) (2007/01/01 2007) 237–241.
[16] B.K. Oelschlager, M. Barreca, L. Chang, C.A. Pellegrini, The use of small intestine submucosa in the repair of paraesophageal hernias: initial observations of a new technique, Am. J. Surg. 186 (1) (Jul 2003) 4–8 (in eng).
[17] D.A. De Ugarte, et al., Mucosal regeneration of a duodenal defect using small intestine submucosa, Am. Surg. 70 (1) (Jan 2004) 49–51 (in eng).

[18] S.A. Alpert, E.Y. Cheng, W.E. Kaplan, W.T. Snodgrass, D.T. Wilcox, B.P. Kropp, Bladder neck fistula after the complete primary repair of exstrophy: a multi-institutional experience, J. Urol. 174 (4 Pt 2) (Oct 2005) 1687–1689. ; discussion 1689-90(in eng).

[19] H.L. Malcarney, F. Bonar, G.A. Murrell, Early inflammatory reaction after rotator cuff repair with a porcine small intestine submucosal implant: a report of 4 cases, Am. J. Sports Med. 33 (6) (Jun 2005) 907–911 (in eng).

[20] R. Demling, J. Niezgoda, G. Haraway, E. Mostow, Small intestinal submucosa wound matrix and full-thickness venous ulcers: preliminary results, Wounds 16 (2004).

[21] C. Zang, et al., Clinical outcomes of a novel porcine small intestinal submucosa patch for full-thickness hand skin defects: a retrospective investigation, J. Orthop. Surg. Res. 18 (1) (Jan 17 2023) 50.

[22] M. Romanelli, V. Dini, M.S. Bertone, Randomized comparison of OASIS wound matrix versus moist wound dressing in the treatment of difficult-to-heal wounds of mixed arterial/venous etiology, Adv. Skin Wound Care 23 (1) (2010).

[23] J.S. Jones, R.R. Rackley, R. Berglund, J.B. Abdelmalak, G. DeOrco, S.P. Vasavada, Porcine small intestinal submucosa as a percutaneous mid-urethral sling: 2-year results, BJU Int. 96 (1) (Jul 2005) 103–106 (in eng).

[24] M.L. Anson, Protein denaturation and the properties of protein groups, in: M. L. Anson, J.T. Edsall (Eds.), Advances in Protein Chemistry, 2, Academic Press, 1945, pp. 361–386.

[25] D.A. Young, D.O. Ibrahim, D. Hu, K.L. Christman, Injectable hydrogel scaffold from decellularized human lipoaspirate, Acta Biomater. 7 (3) (Mar 2011) 1040–1049 (in eng).

[26] B. Falcones, et al., Bioprintable lung extracellular matrix hydrogel scaffolds for 3D culture of mesenchymal stromal cells, Polymers 13 (14) (Jul 18 2021) (in eng).

[27] P.M. Crapo, T.W. Gilbert, S.F. Badylak, An overview of tissue and whole organ decellularization processes, Biomaterials 32 (12) (2011/04/01/2011) 3233–3243.

[28] D.M. Faulk, et al., The effect of detergents on the basement membrane complex of a biologic scaffold material, Acta Biomater. 10 (1) (Jan 2014) 183–193 (in eng).

[29] M.-R. Fan, et al., Tissue engineered esophagus scaffold constructed with porcine small intestinal submucosa and synthetic polymers, Biomed. Mater. 9 (1) (2014/01/23 2014) 015012.

[30] M.S. Kim, H.H. Ahn, Y.N. Shin, M.H. Cho, G. Khang, H.B. Lee, An in vivo study of the host tissue response to subcutaneous implantation of PLGA- and/or porcine small intestinal submucosa-based scaffolds, Biomaterials 28 (34) (2007/12/01/2007) 5137–5143.

[31] M. Nogami, et al., A human amnion-derived extracellular matrix-coated cell-free scaffold for cartilage repair: in vitro and in vivo studies, Tissue Eng. 22 (7–8) (Apr 2016) 680–688 (in eng).

[32] N. Uchida, et al., Nanometer-sized extracellular matrix coating on polymer-based scaffold for tissue engineering applications, J. Biomed. Mater. Res. 104 (1) (2016/01/01 2016) 94–103, https://doi.org/10.1002/jbm.a.35544.

[33] C. Del Gaudio, M. Grigioni, A. Bianco, G. De Angelis, Electrospun bioresorbable heart valve scaffold for tissue engineering, Int. J. Artif. Organs 31 (1) (Jan 2008) 68–75 (in eng).

[34] R.M. Nezarati, M.B. Eifert, D.K. Dempsey, E. Cosgriff-Hernandez, Electrospun vascular grafts with improved compliance matching to native vessels, J. Biomed. Mater. Res. B Appl. Biomater. 103 (2) (2015/02/01 2015) 313–323, https://doi.org/10.1002/jbm.b.33201.

[35] T.W. Buie, et al., Comparative efficacy of resorbable fiber wraps loaded with gentamicin sulfate or gallium maltolate in the treatment of osteomyelitis, J. Biomed. Mater. Res. (2021), https://doi.org/10.1002/jbm.a.37210. (Accessed 5 May 2021).

[36] C.A. Bashur, L.A. Dahlgren, A.S. Goldstein, Effect of fiber diameter and orientation on fibroblast morphology and proliferation on electrospun poly(d,l-lactic-co-glycolic acid) meshes, Biomaterials 27 (33) (2006/11/01/2006) 5681–5688.

[37] C.A. Bashur, R.D. Shaffer, L.A. Dahlgren, S.A. Guelcher, A.S. Goldstein, Effect of fiber diameter and alignment of electrospun polyurethane meshes on mesenchymal progenitor cells, Tissue Eng. 15 (9) (2009/09/01 2009) 2435–2445.

[38] D.S. Puperi, et al., Electrospun polyurethane and hydrogel composite scaffolds as biomechanical mimics for aortic valve tissue engineering, ACS Biomater. Sci. Eng. 2 (9) (2016/09/12 2016) 1546–1558.

[39] K.H. Patel, et al., Aligned nanofibers of decellularized muscle ECM support myogenic activity in primary satellite cells in vitro, Biomed. Mater. 14 (3) (Apr 2 2019) 035010 (in eng).

[40] H. Lee, W. Kim, J. Lee, J.J. Yoo, G.H. Kim, S.J. Lee, Effect of hierarchical scaffold consisting of aligned dECM nanofibers and poly(lactide-co-glycolide) struts on the orientation and maturation of human muscle progenitor cells, ACS Appl. Mater. Interfaces 11 (43) (2019/10/30 2019) 39449–39458.

[41] B.M. Young, et al., Electrospun decellularized lung matrix scaffold for airway smooth muscle culture, ACS Biomater. Sci. Eng. 3 (12) (2017/12/11 2017) 3480–3492.

[42] S. Baiguera, et al., Electrospun gelatin scaffolds incorporating rat decellularized brain extracellular matrix for neural tissue engineering, Biomaterials 35 (4) (2014/01/01/2014) 1205–1214.

[43] R. Deng, et al., Decellularized extracellular matrix containing electrospun fibers for nerve regeneration: a comparison between core–shell structured and preblended composites, Advanced Fiber Materials 4 (3) (2022/06/01 2022) 503–519.

[44] Y. Zhu, et al., Biomimetic hybrid scaffold of electrospun silk fibroin and pancreatic decellularized extracellular matrix for islet survival, J. Biomater. Sci. Polym. Ed. 32 (2) (Feb 2021) 151–165 (in eng).

[45] S. Gao, et al., Fabrication and characterization of electrospun nanofibers composed of decellularized meniscus extracellular matrix and polycaprolactone for meniscus tissue engineering, J. Mater. Chem. B 5 (12) (2017) 2273–2285, https://doi.org/10.1039/C6TB03299K.

[46] N.W. Garrigues, D. Little, J. Sanchez-Adams, D.S. Ruch, F. Guilak, Electrospun cartilage-derived matrix scaffolds for cartilage tissue engineering, J. Biomed. Mater. Res. 102 (11) (Nov 2014) 3998–4008 (in eng).

[47] B. Feng, et al., Engineering cartilage tissue based on cartilage-derived extracellular matrix cECM/PCL hybrid nanofibrous scaffold, Mater. Des. 193 (2020/08/01/2020) 108773.

[48] E. Masaeli, F. Karamali, S. Loghmani, M.B. Eslaminejad, M.H. Nasr-Esfahani, Bio-engineered electrospun nanofibrous membranes using cartilage extracellular matrix particles, J. Mater. Chem. B 5 (4) (2017) 765–776, https://doi.org/10.1039/C6TB02015A.

[49] A. Haider, S. Haider, I.-K. Kang, A comprehensive review summarizing the effect of electrospinning parameters and potential applications of nanofibers in biomedical and biotechnology, Arab. J. Chem. 11 (8) (2018/12/01/2018) 1165–1188.

[50] M.M. Smoak, et al., Fabrication and characterization of electrospun decellularized muscle-derived scaffolds, Tissue Eng. C Methods 25 (5) (2019) 276–287.

[51] M.P. Francis, et al., Electrospinning adipose tissue-derived extracellular matrix for adipose stem cell culture, J. Biomed. Mater. Res. A (7) (2012) 1716–1724, https://doi.org/10.1002/jbm.a.34126vol.100A. (Accessed 1 July 2012).

[52] Y. Ji, et al., Diverse preparation methods for small intestinal submucosa (SIS): decellularization, components, and structure, J. Biomed. Mater. Res. 107 (3) (2019) 689–697.

[53] G.A. Abraham, J. Murray, K. Billiar, S.J. Sullivan, Evaluation of the porcine intestinal collagen layer as a biomaterial, J. Biomed. Mater. Res. 51 (3) (Sep 5 2000) 442–452 (in eng).

[54] T.J. Keane, R. Londono, N.J. Turner, S.F. Badylak, Consequences of ineffective decellularization of biologic scaffolds on the host response, Biomaterials 33 (6) (2012) 1771–1781 (in eng).

[55] B. Brown, K. Lindberg, J. Reing, D.B. Stolz, S.F. Badylak, The basement membrane component of biologic scaffolds derived from extracellular matrix, Tissue Eng. 12 (3) (Mar 2006) 519–526 (in eng).

[56] J.-C. Luo, et al., A multi-step method for preparation of porcine small intestinal submucosa (SIS), Biomaterials 32 (3) (2011/01/01/2011) 706–713.

[57] N. Raval, R. Maheshwari, D. Kalyane, S.R. Youngren-Ortiz, M.B. Chougule, R. K. Tekade, Chapter 10 - importance of physicochemical characterization of nanoparticles in pharmaceutical product development, in: R.K. Tekade (Ed.), Basic Fundamentals of Drug Delivery, Academic Press, 2019, pp. 369–400.

[58] D.D. Cissell, J.M. Link, J.C. Hu, K.A. Athanasiou, A modified hydroxyproline assay based on hydrochloric acid in ehrlich's solution accurately measures tissue collagen content, Tissue Eng. C Methods 23 (4) (Apr 2017) 243–250 (in eng).

[59] I. Arnaoutova, H.K. Kleinman, In vitro angiogenesis: endothelial cell tube formation on gelled basement membrane extract, Nat. Protoc. 5 (4) (2010/04/01 2010) 628–635.

[60] M. Nguyen, Y. Shing, J. Folkman, Quantitation of angiogenesis and antiangiogenesis in the chick embryo chorioallantoic membrane, Microvasc. Res. 47 (1) (Jan 1994) 31–40 (in eng).

[61] S.M. Chau, S.M. Herting, D.A. Noltensmeyer, H. Ahmed, D.J. Maitland, S. Raghavan, Macrophage activation in response to shape memory polymer foam-coated aneurysm occlusion devices, J. Biomed. Mater. Res. B Appl. Biomater. 110 (7) (Jul 2022) 1535–1544 (in eng).

[62] D.A. Donehoo, C.A. Collier, S.N. VandenHeuvel, S. Roy, S.C. Solberg, S. A. Raghavan, Degrees of macrophage-facilitated healing in aneurysm occlusion devices, J. Biomed. Mater. Res. B Appl. Biomater. 112 (2) (Feb 2024) e35385 (in eng).

[63] B. Schoen, et al., Electrospun extracellular matrix: paving the way to tailor-made natural scaffolds for cardiac tissue regeneration, Adv. Funct. Mater. 27 (34) (2017) 1700427.

[64] R. Nezarati, M. Eifert, E. Cosgriff-Hernandez, Effects of humidity and solution viscosity on electrospun fiber morphology, Tissue Eng. C Methods 19 (10) (2013) 810–819.

[65] C. Drew, X. Wang, L.A. Samuelson, J. Kumar, The effect of viscosity and filler on electrospun fiber morphology, J. Macromol. Sci., Part A 40 (12) (2003/01/11 2003) 1415–1422.

[66] P. Gupta, C. Elkins, T.E. Long, G.L. Wilkes, Electrospinning of linear homopolymers of poly(methyl methacrylate): exploring relationships between fiber formation, viscosity, molecular weight and concentration in a good solvent, Polymer 46 (13) (2005/06/17/2005) 4799–4810.

[67] A. Padhi, A.S. Nain, ECM in differentiation: a review of matrix structure, composition and mechanical properties, Ann. Biomed. Eng. 48 (3) (2020/03/01 2020) 1071–1089.

[68] M.C. McCabe, A.J. Saviola, K.C. Hansen, Mass spectrometry-based atlas of extracellular matrix proteins across 25 mouse organs, J. Proteome Res. 22 (3) (Mar 3 2023) 790–801 (in eng).

[69] L. Salvatore, N. Gallo, M.L. Natali, A. Terzi, A. Sannino, M. Madaghiele, Mimicking the hierarchical organization of natural collagen: toward the development of ideal scaffolding material for tissue regeneration, Front. Bioeng. Biotechnol. 9 (2021).

[70] M. Dinkgreve, M. Fazilati, M. Denn, D. Bonn, Carbopol: from a simple to a thixotropic yield stress fluid, J. Rheol. 62 (2018) 773–780.
[71] D. Gupta, M. Jassal, A.K. Agrawal, Electrospinning of poly(vinyl alcohol)-based boger fluids to understand the role of elasticity on morphology of nanofibers, Ind. Eng. Chem. Res. 54 (5) (2015/02/11 2015) 1547–1554.
[72] S.M. Schmalholz, Finite amplitude folding of single layers: elastica, bifurcation and structural softening, Phil. Mag. 86 (21–22) (2006/07/21 2006) 3393–3407.
[73] R. Salehiyan, K. Hyun, Effect of organoclay on non-linear rheological properties of poly(lactic acid)/poly(caprolactone) blends, Kor. J. Chem. Eng. 30 (2013).
[74] J.A. Reid, A. McDonald, A. Callanan, Modulating electrospun polycaprolactone scaffold morphology and composition to alter endothelial cell proliferation and angiogenic gene response, PLoS One 15 (10) (2020) e0240332.
[75] D.G. Han, et al., Optimization of electrospun poly(caprolactone) fiber diameter for vascular scaffolds to maximize smooth muscle cell infiltration and phenotype modulation, Polymers 11 (4) (2019) 643.
[76] S.J. Kim, D.H. Jang, W.H. Park, B.-M. Min, Fabrication and characterization of 3-dimensional PLGA nanofiber/microfiber composite scaffolds, Polymer 51 (6) (2010/03/11/2010) 1320–1327.
[77] Q.P. Pham, U. Sharma, A.G. Mikos, Electrospun poly(ε-caprolactone) microfiber and multilayer nanofiber/microfiber scaffolds: characterization of scaffolds and measurement of cellular infiltration, Biomacromolecules 7 (10) (2006/10/01 2006) 2796–2805.
[78] M.K. Leach, Z.Q. Feng, S.J. Tuck, J.M. Corey, Electrospinning fundamentals: optimizing solution and apparatus parameters, J. Vis. Exp. 47 (Jan 21 2011) (in eng).
[79] R. Rošic, J. Pelipenko, P. Kocbek, S. Baumgartner, M. Bešter-Rogač, J. Kristl, The role of rheology of polymer solutions in predicting nanofiber formation by electrospinning, Eur. Polym. J. 48 (8) (2012/08/01/2012) 1374–1384.
[80] X. Zhang, C. Hu, H.-m. Wu, Z.-g. Ma, Q.-z. Tang, Fibronectin type III domain-containing 5 in cardiovascular and metabolic diseases: a promising biomarker and therapeutic target, Acta Pharmacol. Sin. 42 (9) (2021/09/01 2021) 1390–1400.
[81] I. Valiente-Alandi, et al., Inhibiting fibronectin attenuates fibrosis and improves cardiac function in a model of heart failure, Circulation 138 (12) (Sep 18 2018) 1236–1252 (in eng).
[82] A. Charruyer, M. Silvander, M. Caputo-Janhager, I. Raymond, R. Ghadially, Proderm technology: a water- based lipid delivery system for dermatitis that penetrates viable epidermis and has antibacterial effects, BMC Dermatol. 19 (2019).
[83] B. Forslind, A domain mosaic model of the skin barrier, Acta Derm. Venereol. 74 (1) (Jan 1994) 1–6 (in eng).
[84] C.M. Dobson, Protein folding and misfolding, Nature 426 (6968) (2003) 884–890.
[85] R. Usha, T. Ramasami, The effects of urea and n-propanol on collagen denaturation: using DSC, circular dicroism and viscosity, Thermochim. Acta 409 (2) (2004/01/30/2004) 201–206.
[86] T. Palmosi, et al., Small intestinal submucosa-derived extracellular matrix as a heterotopic scaffold for cardiovascular applications, Frontiers in Bioengineering and Biotechnology, Original Research 10 (2022).
[87] C.-A. Dai, Y.-F. Chen, M.-W. Liu, Thermal properties measurements of renatured gelatin using conventional and temperature modulated differential scanning calorimetry, J. Appl. Polym. Sci. 99 (4) (2006/02/15 2006) 1795–1801.
[88] J.K.P. Weder, H.D. Belitz, PROTEIN | chemistry, in: B. Caballero (Ed.), Encyclopedia of Food Sciences and Nutrition, second ed., Academic Press, Oxford, 2003, pp. 4805–4818.
[89] C. Frantz, K.M. Stewart, V.M. Weaver, The extracellular matrix at a glance, J. Cell Sci. 123 (Pt 24) (Dec 15 2010) 4195–4200 (in eng).
[90] J. Casale, J.S. Crane, Biochemistry, glycosaminoglycans, in: *StatPearls*Treasure Island (FL) Ineligible Companies. Disclosure: Jonathan Crane Declares No Relevant Financial Relationships with Ineligible Companies, StatPearls Publishing Copyright © 2024, StatPearls Publishing LLC., 2024.
[91] X. Lin, M. Robinson, T. Petrie, V. Spandler, W.D. Boyd, C.S. Sondergaard, Small intestinal submucosa-derived extracellular matrix bioscaffold significantly enhances angiogenic factor secretion from human mesenchymal stromal cells, Stem Cell Res. Ther. 6 (1) (2015/09/07 2015) 164.
[92] B. Yang, L. Zhou, Z. Sun, R. Yang, Y. Chen, Y. Dai, In vitro evaluation of the bioactive factors preserved in porcine small intestinal submucosa through cellular biological approaches, J. Biomed. Mater. Res. 93A (3) (2010) 1100–1109, https://doi.org/10.1002/jbm.a.32534. (Accessed 1 June 2010).
[93] S. Liu, et al., Synergistic angiogenesis promoting effects of extracellular matrix scaffolds and adipose-derived stem cells during wound repair, Tissue Eng. 17 (5–6) (2011/03/01 2010) 725–739.
[94] I. Moreno-Jiménez, J.M. Kanczler, G. Hulsart-Billstrom, S. Inglis, R.O.C. Oreffo, The chorioallantoic membrane assay for biomaterial testing in tissue engineering: a short-term in vivo preclinical model, Tissue Eng. C Methods 23 (12) (2017/12/01 2017) 938–952.
[95] B.A. Corliss, M.S. Azimi, J.M. Munson, S.M. Peirce, W.L. Murfee, Macrophages: an inflammatory link between angiogenesis and lymphangiogenesis, Microcirculation 23 (2) (2016) 95–121 (in eng).
[96] N. Jetten, S. Verbruggen, M.J. Gijbels, M.J. Post, M.P.J. De Winther, M.M.P. C. Donners, Anti-inflammatory M2, but not pro-inflammatory M1 macrophages promote angiogenesis in vivo, Angiogenesis 17 (1) (2014/01/01 2014) 109–118.
[97] E. Saino, et al., Effect of electrospun fiber diameter and alignment on macrophage activation and secretion of proinflammatory cytokines and chemokines, Biomacromolecules 12 (5) (2011/05/09 2011) 1900–1911.
[98] H. Cao, K. Mchugh, S.Y. Chew, J.M. Anderson, The topographical effect of electrospun nanofibrous scaffolds on the in vivo and in vitro foreign body reaction, J. Biomed. Mater. Res. 93A (3) (2010) 1151–1159.
[99] F. Zhang, et al., TGF-β induces M2-like macrophage polarization via SNAIL-mediated suppression of a pro-inflammatory phenotype, Oncotarget 7 (2016) 52294–52306.
[100] H. Ramirez, S. Patel, I. Pastar, The role of TGFβ signaling in wound epithelialization, Adv. Wound Care 3 (7) (2014) 482–491.
[101] B. Dong, O. Arnoult, M.E. Smith, G.E. Wnek, Electrospinning of collagen nanofiber scaffolds from benign solvents, Macromol. Rapid Commun. 30 (7) (2009/04/01 2009) 539–542, https://doi.org/10.1002/marc.200800634.
[102] C.Z. Mosher, et al., Green electrospinning for biomaterials and biofabrication, Biofabrication 13 (3) (2021) 035049.